Resource

Cell

A Genome-wide CRISPR Screen in Primary Immune Cells to Dissect Regulatory Networks

Graphical Abstract

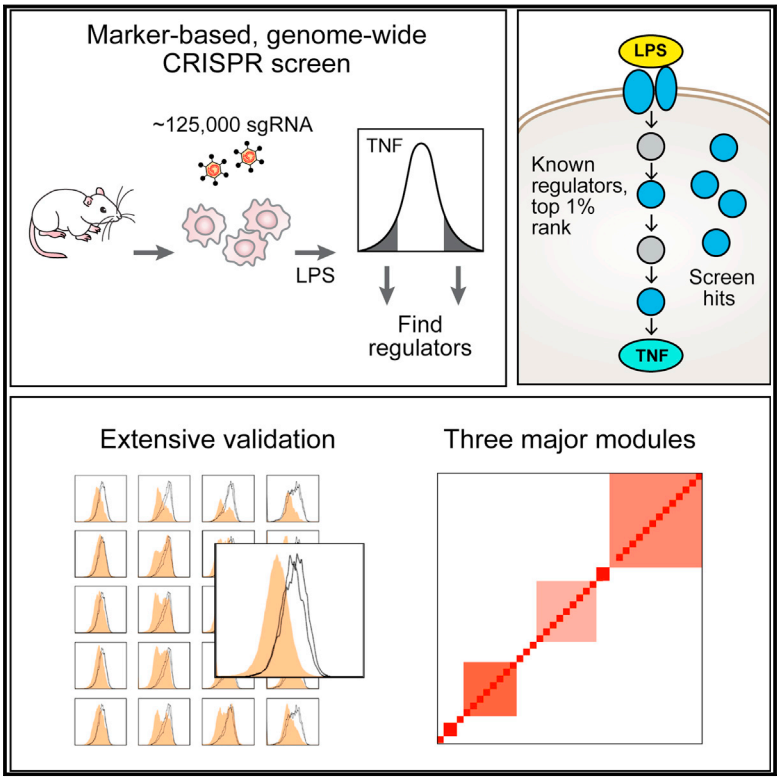

Authors

Oren Parnas, Marko Jovanovic, Thomas M. Eisenhaure, ..., Feng Zhang, Nir Hacohen, Aviv Regev

Correspondence

nhacohen@broadinstitute.org (N.H.), aregev@broadinstitute.org (A.R.)

In Brief

A protein marker-based, genome-wide CRISPR screen has been developed in primary immune cells to identify genes that control the induction of tumor necrosis factor. Many of the known regulators, as well as dozens of previously unknown candidates, have been identified, individually validated, and classified into three functional modules.

Highlights

- Cytokine stain readout for genome-wide CRISPR screen in primary immune cells
- Individual validation of dozens of known and novel regulators of the LPS response
- Regulators cluster into three modules by knockout effect on expression
- General multi-pronged approach to CRISPR screens

Accession Numbers

GSE67164

Parnas et al., 2015, Cell *162*, 1–12
July 30, 2015
http://dx.doi.org/10.1016/j.cell.2015.06.059

CellPress

Please cite this article in press as: Parnas et al., A Genome-wide CRISPR Screen in Primary Immune Cells to Dissect Regulatory Networks, Cell (2015), http://dx.doi.org/10.1016/j.cell.2015.06.059

Cell

A Genome-wide CRISPR Screen in Primary Immune Cells to Dissect Regulatory Networks

Oren Parnas,[1,14] Marko Jovanovic,[1,14] Thomas M. Eisenhaure,[1,2,14] Rebecca H. Herbst,[1,3] Atray Dixit,[1,4] Chun Jimmie Ye,[5] Dariusz Przybylski,[1] Randall J. Platt,[1,6,7,8] Itay Tirosh,[1] Neville E. Sanjana,[1,6,8,9] Ophir Shalem,[1,6] Rahul Satija,[10,11] Raktima Raychowdhury,[1] Philipp Mertins,[1] Steven A. Carr,[1] Feng Zhang,[1,6,7,8,9] Nir Hacohen,[1,2,12,15,*] and Aviv Regev[1,13,15,*]

[1]Broad Institute of MIT and Harvard, Cambridge, MA 02142, USA
[2]Center for Immunology and Inflammatory Diseases, Massachusetts General Hospital, Charlestown, MA 02129, USA
[3]Department of Systems Biology, Harvard Medical School, Boston, MA 02114, USA
[4]Harvard-MIT Division of Health Sciences and Technology, Cambridge, MA 02139, USA
[5]Institute for Human Genetics, Department of Epidemiology and Biostatistics, Department of Bioengineering and Therapeutic Sciences, University of California, San Francisco, San Francisco, CA 94143, USA
[6]McGovern Institute for Brain Research, Massachusetts Institute of Technology, Cambridge, MA 02139, USA
[7]Department of Brain and Cognitive Sciences, Massachusetts Institute of Technology, Cambridge, MA 02139, USA
[8]Department of Biological Engineering, Massachusetts Institute of Technology, Cambridge, MA 02139, USA
[9]Stanley Center for Psychiatric Research, Broad Institute of MIT and Harvard, Cambridge, MA 02142, USA
[10]New York Genome Center, New York, NY 10013, USA
[11]New York University, Center for Genomics and Systems Biology, New York, NY 10012, USA
[12]Department of Medicine, Harvard Medical School, Boston MA 02114
[13]Department of Biology, Howard Hughes Medical Institute, Massachusetts Institute of Technology, Cambridge, MA 02140, USA
[14]Co-first author
[15]Co-senior author
*Correspondence: nhacohen@broadinstitute.org (N.H.), aregev@broadinstitute.org (A.R.)
http://dx.doi.org/10.1016/j.cell.2015.06.059

SUMMARY

Finding the components of cellular circuits and determining their functions systematically remains a major challenge in mammalian cells. Here, we introduced genome-wide pooled CRISPR-Cas9 libraries into dendritic cells (DCs) to identify genes that control the induction of tumor necrosis factor (Tnf) by bacterial lipopolysaccharide (LPS), a key process in the host response to pathogens, mediated by the Tlr4 pathway. We found many of the known regulators of Tlr4 signaling, as well as dozens of previously unknown candidates that we validated. By measuring protein markers and mRNA profiles in DCs that are deficient in known or candidate genes, we classified the genes into three functional modules with distinct effects on the canonical responses to LPS and highlighted functions for the PAF complex and oligosaccharyltransferase (OST) complex. Our findings uncover new facets of innate immune circuits in primary cells and provide a genetic approach for dissection of mammalian cell circuits.

INTRODUCTION

Regulatory circuits that control gene expression in response to extracellular signals perform key information processing roles in mammalian cells, but their systematic unbiased reconstruction remains a fundamental challenge. There are currently two major strategies for associating targets with their putative regulators on a genomic scale (reviewed in Kim et al., 2009): (1) observational (correlative) approaches that relate them based on statistical dependencies in their quantities or physical associations and (2) perturbational (causal) approaches that relate them by the effect that a perturbation in a putative regulator has on its target.

While observational strategies have become a cornerstone of circuit inference from genomic data, perturbational strategies have been more challenging to apply on a genomic scale, especially in primary mammalian cells. RNAi, which until recently was the main tool available in mammals, is limited by off-target effects and lack of sufficient suppression of expression (Echeverri et al., 2006), whereas more effective strategies based on haploid cell lines (Carette et al., 2009) are not applicable to the diversity of primary cell types and their specialized circuitry. As a result, a hybrid approach has emerged (Amit et al., 2011), where genomic profiles (e.g., of mRNAs, protein-DNA binding, protein levels, protein phosphorylation, etc.) are used to build observational models from which a smaller set of dozens of candidate regulators are identified. These candidates are in turn tested by perturbation.

The recent introduction of genome editing in mammalian cells using the clustered, regularly interspaced, short palindromic repeats (CRISPR)-associated nuclease Cas9 system has enabled pooled genome-wide screens of gene function (Gilbert et al., 2014; Konermann et al., 2015; Shalem et al., 2014; Wang et al.,

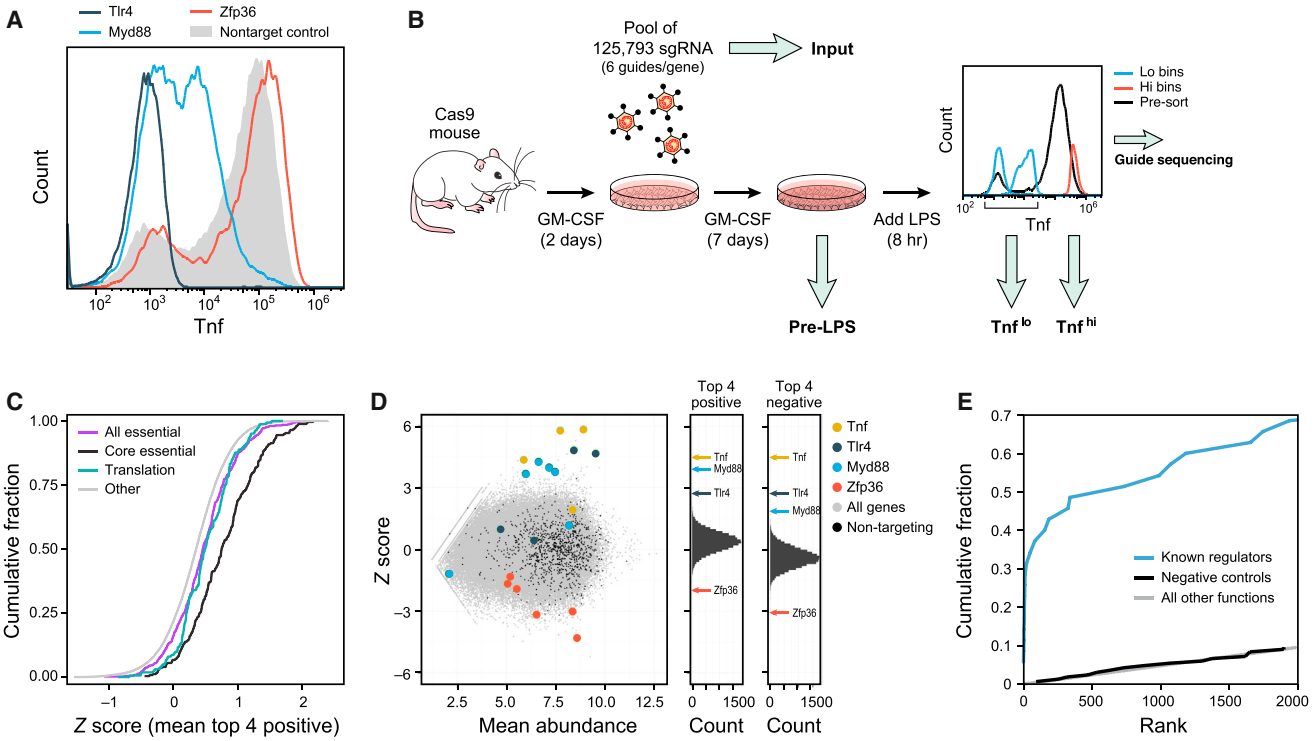

Figure 1. A Genome-wide Pooled CRISPR Screen in Mouse Primary DCs

(A) Flow cytometry of intracellular Tnf levels following 8 hr of LPS stimulation for single sgRNAs.

(B) Design of a genome-wide CRISPR screen.

(C) Cumulative distribution function (CDF) plots of the gene level Z-score distribution of genes annotated as "essential" (purple) and "core essential" (black) in Hart et al. (2014), "translation" (in GO, blue), and all other genes (gray).

(D) (Left) Binned Z scores (ZS) of the Tnf^{lo}/Tnf^{hi} ratios (y axis) versus sgRNA mean abundances in Tnf^{lo} and Tnf^{hi} (x axis). (Right) Gene score distribution for positive (ZS) and negative (ZS) regulators (Experimental Procedures).

(E) CDFs of screen ranks for the 35 genes in the TLR pathway from LPS to Tnf (KEGG, blue), non-targeting controls (black), and all other genes (gray).

See also Figure S1.

2014). In such screens, pooled libraries are introduced into cell lines and cellular phenotypes are selected based on cell lethality or growth. To expand the biological processes that can be studied, there remains a need to adapt these methods for short-term primary cell cultures and selecting cellular phenotypes based on more versatile molecular markers.

Here, we present a pooled CRISPR strategy to dissect the innate immune response of bone-marrow-derived dendritic cells (BMDCs, or DCs) isolated from Cas9-expressing transgenic mice. Building on our recent observation that lentiviruses expressing single-guide RNAs (sgRNAs) could be used to knock out genes in these cells (Platt et al., 2014), we infected DCs with a pooled, genome-wide library of lentiviruses, stimulated them with lipopolysaccharide (LPS), and monitored their responses by intra-cellular staining for the inflammatory cytokine Tnf, a major marker of the early response to LPS. We used flow cytometry to isolate cells that failed to fully induce Tnf or that induced it more strongly, and then we determined sgRNA abundance by deep sequencing. We recovered many of the key known regulators of TLR signaling, validated dozens of new regulators, and identified three functional modules of regulators with distinct regulatory effects. Our study identifies new facets in the complex response of immune cells to pathogens and provides a general strategy for systematically dissecting circuits in other primary mammalian cells.

RESULTS

A System for Cell-Autonomous, Pooled Genetic Screens in BMDCs Derived from Cas9-Expressing Mice

To enable genome-wide pooled genetic screens, we developed a cell-autonomous readout of innate immune activation by intracellular staining of a central inflammatory cytokine, Tnf. To test the assay, we individually transduced BMDCs with lentiviruses expressing sgRNAs (Experimental Procedures) that target each of three genes: (1) *Tlr4*, the cell membrane receptor that senses bacterial LPS; (2) *Myd88*, a key component required for Tlr4 signaling to induce Tnf; and (3) *Zfp36* (TTP), an RNA-binding protein that destabilizes Tnf mRNA. Following LPS activation, we added Brefeldin A to block Tnf secretion and at 8 hr post-activation detected Tnf with a fluorescent antibody using flow cytometry. Compared to a non-targeting sgRNA control, sgRNAs targeting *Myd88* or *Tlr4* strongly reduced Tnf, whereas sgRNAs targeting *Zfp36* increased Tnf (Figure 1A). These results provide

an experimental system in BMDCs for an autonomous genome-wide pooled screen based on cell sorting.

A Genome-wide Pooled sgRNA Library Screen in Primary BMDCs

We performed three independent, pooled genome-wide screens using a library of lentiviruses harboring 125,793 sgRNAs targeting 21,786 annotated protein-coding and miRNA mouse genes (Sanjana et al., 2014), as well as 1,000 non-targeting sgRNA as negative controls. In each of the three replicate screens, we infected 60–200 million BMDCs with the library at a multiplicity of infection (MOI) of 1, stimulated cells with LPS, and sorted Cd11c+ cells based on high or low Tnf expression levels (~5 million cells/bin; Figure 1B and Experimental Procedures). We then amplified and sequenced sgRNAs from four sources (Figure 1B, thick gray arrows): post-LPS cells with (1) high Tnf ("Tnf^{hi}") or with (2) low Tnf ("Tnf^{lo}"), (3) cells from the last day of differentiation prior to LPS stimulation (day 9, "pre-LPS"), and (4) plasmid DNA of the input lentiviral library ("Input"). We reasoned that sgRNAs against positive regulators of Tnf expression would be enriched in Tnf^{lo} relative to Tnf^{hi}, that sgRNAs targeting negative regulators will be enriched in Tnf^{hi} relative to Tnf^{lo}, and that sgRNAs targeting genes essential for DC viability or differentiation would be depleted in pre-LPS compared to Input. We established two computational methods to address the inherent noise of the screen (Figure S1A): the first using Z scores (ZS) of the fold change in normalized sgRNA abundance (and then averaging the top four sgRNAs per gene) and the second analogous to differential expression (DE) analysis of sequenced RNA (Love et al., 2014; Experimental Procedures). The top-ranked genes substantially overlap between the two approaches (50/100 for positive regulators, 30/100 for negative regulators, $p < 10^{-10}$, hypergeometric test), and their rankings are well correlated (Figures S1B and S1C) up to ranks 150 and 50 for positive and negative regulators, respectively (Figures S1D and S1E). While our screen is in principle compatible with discovery of both positive and negative regulators, it was conducted at high (near-saturation) levels of LPS and is thus likely to be less sensitive for discovery of negative regulators due to limited dynamic range for observing further Tnf induction.

The Screen Correctly Identifies Known Regulators of Cell Viability, Differentiation, Tnf Expression, and Tlr4 Signaling

To assess the initial quality of our screen and scoring scheme, we first determined that, as expected, sgRNAs against "essential" genes (Hart et al., 2014) were depleted in pre-LPS samples compared to Input (Figure 1C, Figure S1F, and Table S1).

Next, a comparison of sgRNAs between Tnf^{hi} and Tnf^{lo} was also consistent with our predictions, with sgRNAs targeting known positive regulators of the response (e.g., *Tlr4* and *Myd88*) being enriched in Tnf^{lo} compared to Tnf^{hi} and those targeting negative regulators (e.g., *Zfp36*) being depleted in Tnf^{lo} (ZS analysis, Figure 1D and Table S1; DE analysis, Figure S1G and Table S1). The top-ranked genes were highly enriched for those annotated as responsive to LPS (the highest-scoring category; GOrilla, false discovery rate [FDR] q val = 10^{-12}; Eden et al., 2009) or assigned to the Tlr4-to-Tnf pathway (in KEGG; Kanehisa and Goto, 2000, Figure 1E, and Experimental Procedures); they were also far more likely to be expressed (Figure S1H, e.g., 78% of the top 169 genes, compared to 44% of all genes; $p = 10^{-16}$, hypergeometric test) at higher levels ($p = 10^{-6}$ Kolmogorov-Smirnov [KS] test) and were more likely to be differentially expressed by RNA-seq following LPS stimulation (Experimental Procedures and Table S1).

The top 10 ranked positive regulator genes were almost exclusively populated by the hallmark members of TLR signaling, with many others among the top 100, showing that an unbiased, genome-wide screen can decipher near-complete pathways (Figure 2B and Table S1). Tnf had the top rank, demonstrating the screen's quantitative nature. Key regulators of the LPS response with high ranks in our screen included (Figure 2B): *Tlr4* (rank 10) and its co-receptors *Ly96* (MD2) (rank 2) and *Cd14* (rank 3); well-known members of LPS/Tlr4 signaling, including *Ticam2* (TRAM, rank 5), *Ticam1* (TRIF, rank 8), *Myd88* (rank 4), *Tirap* (rank 9), and *Traf6* (rank 13); *Rela* (rank 11), a component of NF_KB, which regulates Tnf transcription; and two regulators of NF_KB: *Ikbkb* and *Ikbkg* (NEMO) (rank 23 and rank 84, respectively). Other notable known regulators of the immune response and DC function include the DC pioneer transcription factor *Cebpb* (rank 21), *Akirin2* (rank 39), and *Rnf31* (rank 42) and *Rbck1* (rank 19), two subunits of the linear ubiquitin chain assembly complex (LUBAC) that tags NEMO and enables NFKB activation. Overall, the top 100 ranked genes were highly enriched for central genes in the LPS-to-Tnf pathway, as annotated by KEGG (13/35 annotated genes are in the top 100; $p = 10^{-22}$, hypergeometric test) (Figure 1E).

Dozens of Positive Regulators Identified by the Screen Validated Using Individually Cloned sgRNAs

To validate the top genes in the ranked list, we next tested two to three sgRNAs against each of the top 176 (112 positive and 64 negative) ranked candidate regulators in individual, rather than pooled, assays, along with 53 non-targeting controls. We measured intracellular Tnf levels by flow cytometry (Figure 2A), excluding sgRNAs with significant reduction in viability (Table S2 and Experimental Procedures).

Overall, we verified 57 positive regulators out of 112 tested: 45 with at least two independent sgRNAs and another 12 genes with one sgRNA (Figure 2C and Table S1), including key known regulators (Figure 2B, right). The rate of true-positive regulators was in agreement with our predicted FDR (Figure 2E), and the effect size of TNF phenotype was well correlated with the original ranking (Figure 2D), supporting the accuracy of our statistical framework. Notably, 27 out of 57 validated genes are not previously annotated for immune function or Tnf regulation (e.g., *Midn*; Experimental Procedures and Table S1).

We explored the basis for false negatives among the positive regulators by examining 15 known regulators of LPS activation that were not among the top 100 ranked genes in the screen. Using 28 additional sgRNAs, we found that 8 of the 15 known regulators indeed reduced Tnf levels (Figures S2A and S2B; notably, these eight were better ranked in the original screen (187–4,417) than the remaining seven genes (2,871–18,314), demonstrating that some factors outside of our threshold still have functional impact in this complex response.

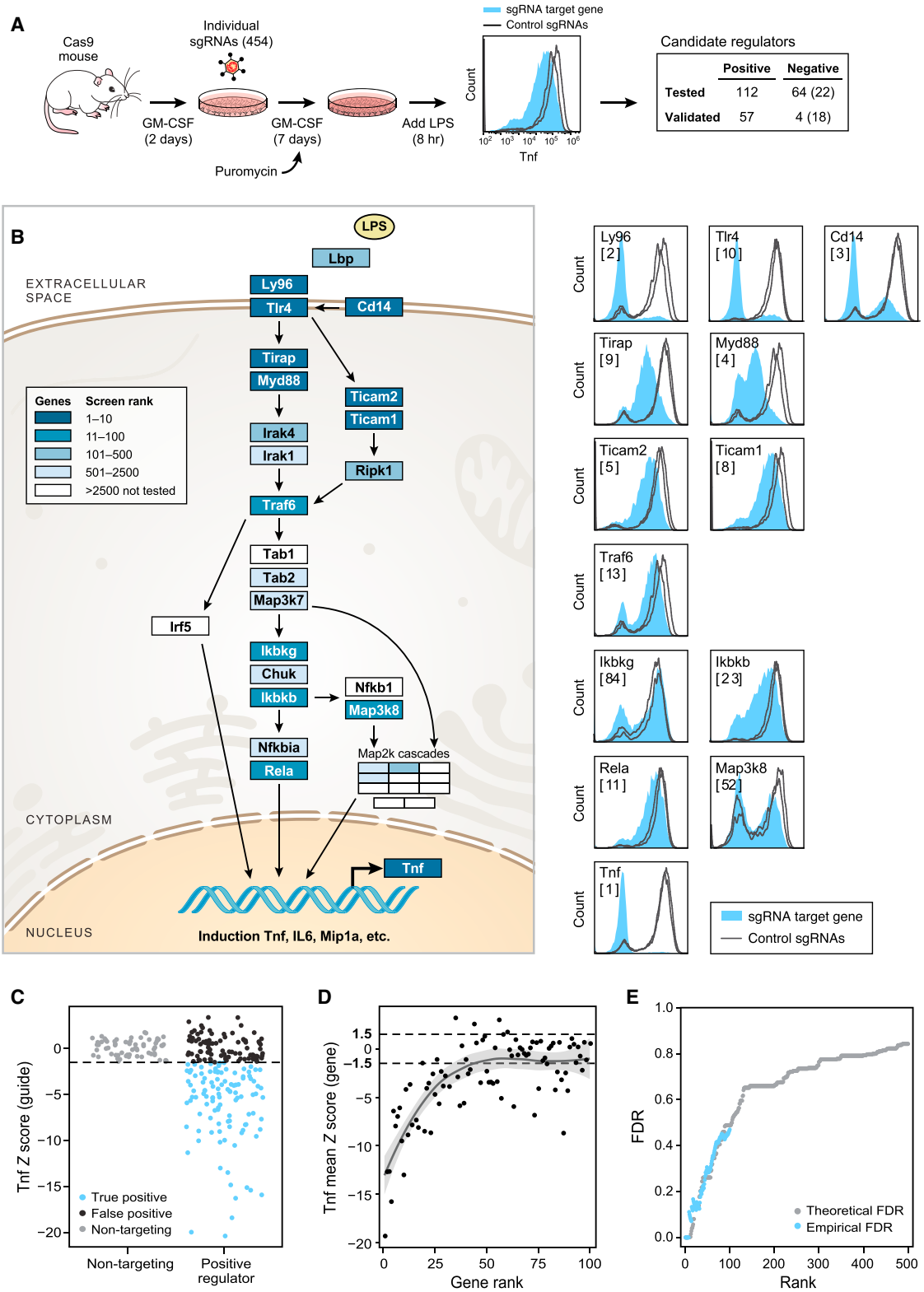

Figure 2. Individual sgRNAs Verify Dozens of Top Hits from the Pooled Screen

(A) Experimental design to validate top screen hits by individual sgRNA knockouts. Tnf levels were measured by flow cytometry for each sgRNA (filled) versus control sgRNAs (lines). (Right) The numbers of positive and negative candidate regulators tested and verified using 100 ng/ml or, in parentheses, 20 ng/ml LPS.

(legend continued on next page)

Optimized Characterization of Novel Negative Regulators by Analysis at Unsaturated Levels of Tnf

Only 4 of 64 (Figure S2C and Table S1) putative negative regulators were initially validated by two independent sgRNAs, including: *Zfp36* (rank 1 among the ZS negative regulators; Figure 1A), *Stat5b* (rank 9), *Pdcd10* (CCM3, rank 32), and *Ppp2r1a* (rank 16). Each of these, including *Zfp36*, our known control, associates with human disease. Stat5b, a transcription factor activated in response to cytokine induction (Darnell, 1997), is important for DC differentiation (Sebastián et al., 2008) (consistent with a low-Cd11c phenotype in its targeted cells; Figure S2E) but was not previously implicated in regulation of Tnf. Pdcd10 (CCM3) was not previously reported to regulate Tnf and is associated with familial cerebral cavernous malformation (CCM) (Faurobert and Albiges-Rizo, 2010), a vascular pathological condition. Pdcd10 (CCM3) was also found to physically interact with Ppp2r1a, the fourth negative regulator (Goudreault et al., 2009). Interestingly, Calyculin A, a drug that inhibits the protein phosphatase 1 and protein phosphatase 2A complexes, of which Ppp2r1a is a member, was previously shown to induce Tnf secretion (Boehringer et al., 1999).

The small proportion of validated negative regulators and their relatively subtle phenotype suggested that our screen, conducted with a high (100 ng/ml) LPS concentration that leads to near-saturated Tnf levels, may be less sensitive for further induction of Tnf when perturbing negative regulators. To increase sensitivity for negative regulators, we reduced LPS by 5-fold and observed higher Tnf for 24 of 37 (65%) retested sgRNAs targeting 22 genes, including the translation initiation factor *Eif5* not previously associated with TNF regulation, and the Rela-homolog DNA-binding protein *Dnttip1* (TdIF1) (Yamashita et al., 2001) (Figure S2D). While this test is different from the initial screen and thus cannot assess its FDR, it does provide additional functional regulators.

A Deeper Secondary Pooled Screen Uncovers Additional Regulators with Greater Sensitivity and Specificity

To reduce false negatives due to limited cell numbers relative to the size of the sgRNA library or to sgRNA design, we performed a secondary pooled screen targeting 2,569 of the top genes (Table S5) from the genome-wide screen with 10 sgRNAs per gene (using the improved design of Doench et al. [2014]) and 4.9-fold more cells per sgRNA. The secondary screen showed greater specificity and sensitivity, as reflected in enrichment of the known regulators (Figures S2F and S2G), highly correlated ranking of hits from the Z score and DE analyses (Figure S2H and Table S1), and reduced FDR compared to the genome-wide screen (e.g., FDR = 6.7% for top 100 genes, Figure S2I), indicating a reduction in noise and enrichment for true positives. The hits included: *Irak4* (ranked 9 in the secondary screen versus 187 in the primary screen), *Irak1* (60 versus 992), *Sharpin* (another subunit of the LUBAC complex, ranked 36), and *Nedd8* (ranked 52) and its E2 conjugation enzyme, *Ube2f* (ranked 25). In the secondary screen, we found 19 positive regulators with no immune annotation that were not found in the primary screen ($Z > 1.5$; FDR = 0.094; Table S1; e.g., *Gpatch8*). A deeper secondary screen is thus an effective strategy for increasing the rate of true positives when it is not feasible to expand the primary screen.

Positive Tnf Regulators Are Organized in Functional Modules by Their Impact on RNA and Protein Expression

While all of the validated regulators affect Tnf levels, the pathways and mechanisms through which they act may be distinct. To help determine those, we first measured the impact of the validated positive regulators on the expression of four additional protein markers (Experimental Procedures), each reflecting distinct facets of DC biology: Cd11c (the defining surface marker of BMDCs), Cd14 (a Tlr4 co-receptor), Mip1α (an induced chemokine), and Il6 (an induced inflammatory cytokine). We statistically tested the effect of each sgRNA on protein expression compared to a set of six to eight non-targeting controls (Figure S3A and Experimental Procedures) and then grouped genes based on the similarity of their effects (Figures 3A, 3B, and Table S2). Notably, the Tnf distribution varied from unimodal to bimodal across different targeted genes (Figure 2B); sequencing several target genes showed that, in some but not all cases, this could be explained by the proportion of edited cells (Figures S4A–S4C).

The genes are largely partitioned into three major modules (Figure 3A). Module I consisted of sgRNAs targeting 17 genes, including 9 canonical regulators validated in the screen, each reducing the levels of Cd14 and Il6, but not Cd11c (Figures 3A–3C and Table S2), consistent with the roles of the known regulators in LPS signaling. Additional module members (Figure 3A) included: *Ctcf*, previously implicated in DC differentiation and activation (Koesters et al., 2007) and Tnf expression (Nikolic et al., 2014), and the miRNA mmu-mir-106a, a member of the microRNA-17/20a family. Module II included nine regulators whose sgRNAs reduced all four proteins, among them: four subunits of the OST protein glycosylation complex (see below), *Alg2*, a glycosyltransferase involved in oligosaccharide synthesis (Haeuptle and Hennet, 2009; Huffaker and Robbins, 1983), and genes whose molecular functions are currently unknown, such as *Tmem258* (Figure 3A). Module III consisted of sgRNAs targeting three subunits of the PAF complex and Pol2rg; each reduced Cd11c and Il6 expression but had a very minor, albeit consistent, effect on Mip1α (Figures 3B and 3C) and no effect on CD14. Some genes were not part of the three modules, including *Midn*, which is encoded in a locus associated with ulcerative

(B) (Left) All components of the TLR pathway (KEGG) linking LPS and Tnf and their ranks in the genome-wide screen (blue scale). (Right) Intracellular Tnf levels for each targeted gene (filled) compared to sgRNA controls (lines).

(C) The intracellular Tnf signal (sgRNA Z score relative to non-targeting sgRNA) of candidate positive regulators (right) and non-targeting controls (left). (Blue) Validated hits.

(D) Mean Tnf Z score for all sgRNAs targeting the same gene at each screen rank. Dark gray line indicates LOESS regression (local regression curve), 95% confidence interval shown in gray.

(E) Theoretical (gray) and empirical (blue) FDR by screen rank.

See also Figure S2.

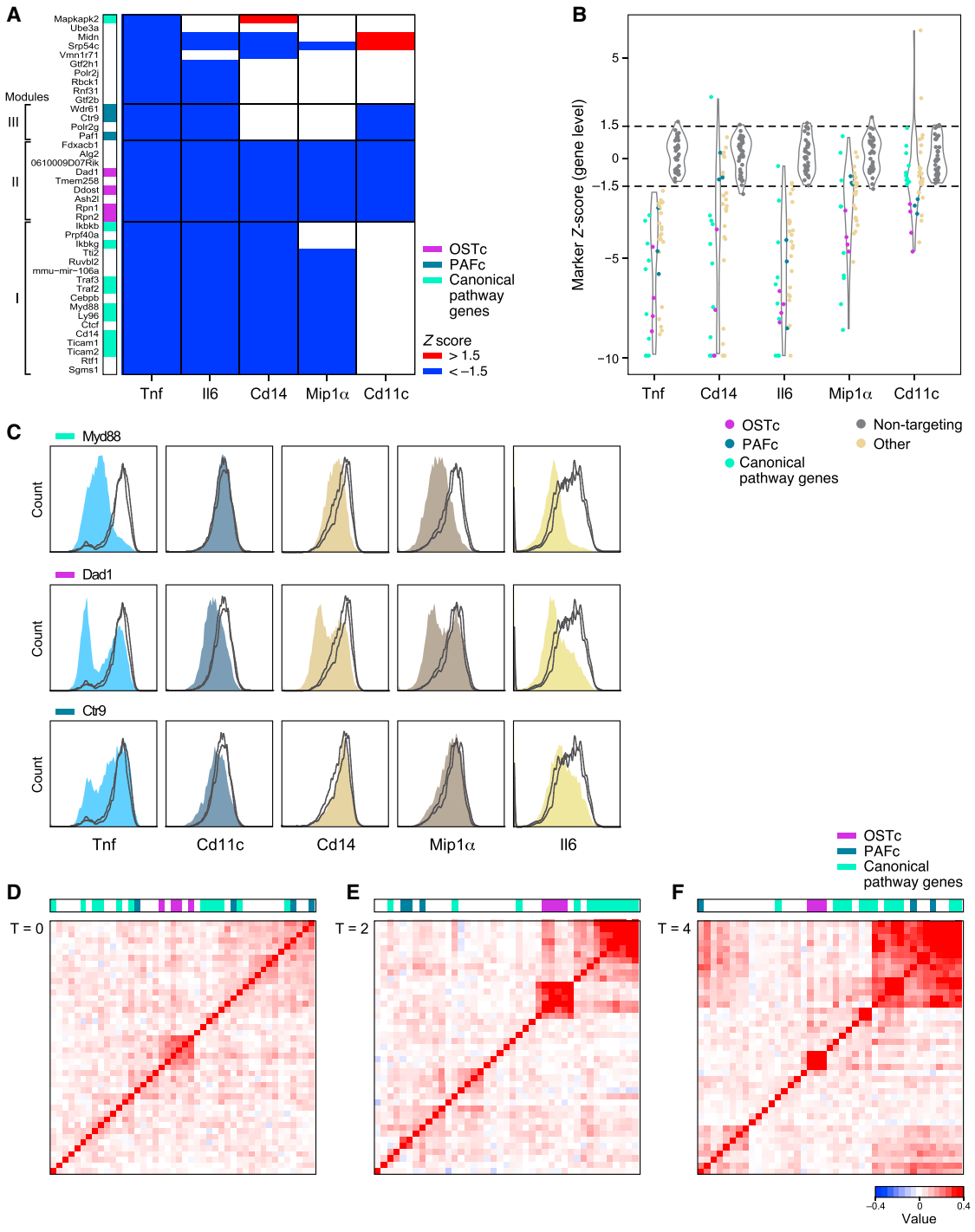

Figure 3. The Validated Positive Regulators Partition into Key Modules by Their Effect on Protein and RNA Expression

(A) Change in expression (blue, reduced; red, increased; Z score) of five protein markers (labeled columns) measured by flow staining with antibodies (Experimental Procedures) for cells with sgRNAs targeting the indicated genes (rows). Three modules indicated with brackets, and color bar on left corresponds to legend on right.

(B) Violin plots of the distribution of Z scores of true positive regulators of Tnf (left) or of non-targeting control sgRNAs (right) for each marker. Functional groups are colored as in (A).

(C) Effects of selected sgRNAs targeting genes in each of three modules on protein markers for true positives (filled) versus non-targeting controls (lines).

(D–F) Correlation of global RNA expression profiles (normalized to non-targeting control values) for verified positive regulators per time point post-LPS, as indicated. Color scale: Pearson correlation coefficient.

See also Figure S3.

colitis (based on GWAS studies; Beck et al., 2014) but has no known molecular function.

Regulators in each of the modules may affect Tnf levels through mechanisms that are shared by members of the same module but are distinct from those of the other modules. To further assess this, we next measured with RNA-seq the global effects of each regulator on mRNA levels at 0, 2, 4, and 6 hr post-LPS (without Brefeldin), compared to 12–14 non-targeting sgRNAs per time point (Figures 3D–3F, S3B–S3E, and Experimental Procedures). Grouping regulators into modules based on similarity in their profiles, we found that the modules change over time, with the distinctions sharpened earlier in the response and diminishing at later time points as they converge through likely indirect effects. Pre-LPS (t = 0 hr, Figure 3D), most regulators show little effect compared to non-targeting controls, except for one group consisting almost entirely of members of the OST complex, as well as *Alg2* and *Tmem258*. At 2 and 4 hr (Figures 3E and 3F), the regulators partition to several modules, including the known TLR regulators, a PAF complex module, and a module associated with RNA regulators including *Akirin2*, *Polr2g*, and *Pabpc1*. Perturbation of the genes in the latter module reduces ($p < 0.001$) the expression of genes involved in immune effector processes and reduces regulation of immune system processes (GOrilla qFDR 0.0377 and 0.0246, respectively, at t = 2 hr; Table S3). By 6 hr (Figure S3E), the transcriptional effect of most regulators is more similar. Notably, addition of Brefeldin in these profiling experiments does not affect Tnf expression, suggesting that the effect of gene perturbation in the screen versus the profiling experiment is comparable for inflammatory gene expression (Figure S3F).

Taken together, our data suggest three key modules that impact Tnf levels in distinct ways. We next explored these, focusing on the modules of the OST and PAF complexes.

Components of the OST Complex and the ER Folding and Translocation Pathway Are Important for Tnf Expression in Response to LPS

Among the 57 genes that were confirmed individually were four structural subunits of the nine-protein oligosaccharyltransferase complex (OSTc): *Dad1*, *Ddost*/OST48, *Rpn1*, and *Rpn2*. Consistent with their physical association, they were all members of the same protein- and RNA-defined modules (Figures 3A and 3D–3F). The ER-resident OSTc tags asparagine residues of newly translated proteins with oligosaccharide chains that are critical for protein folding and transport through the ER. At least six other genes essential for the ER transport pathway (*Alg2*, *Srpr*, *Srp54c*, *Sec61*, *Hsp90b*, and *Sec13*; Figure 4A), upstream or downstream of OSTc, were also among the top-ranking validated positive regulators (although not necessarily in the OSTc module).

More than 2,300 proteins are known to be N-glycosylated (Zielinska et al., 2010), and knocking out subunits of OSTc may affect Tnf levels directly or indirectly and—in either case—could reflect a more global effect on N-glycosylated proteins and cell phenotype in LPS-stimulated BMDCs. Since both Ly96 and Tlr4 are N-glycosylated and Tlr4 transport to the membrane is disrupted in the absence of tagged asparagines (da Silva Correia and Ulevitch, 2002), we hypothesized that OSTc could affect Tnf levels by impacting Tlr4 and/or its signaling. Indeed, targeting any of the four OSTc structural subunits or *Alg2* (Figures 3C and S4D) strongly reduced each of the four protein markers (Figure 3A), including CD11c. This general reduction is consistent with either of two hypotheses: (1) the cells are not properly differentiated, or (2) the cells have differentiated properly but their LPS sensing is compromised. In the latter case, OSTc mutants could have either (a) a global signaling defect (e.g., due to a lack of key membrane receptors) or (b) a more specific regulatory effect.

To distinguish between these hypotheses, we examined the specific genes whose expression is affected in OSTc-targeted cells, compared to cells targeted by known regulators from the TLR pathway, or in cells with non-targeting sgRNA controls, either before or after LPS stimulation (Figures 4B–4E and Experimental Procedures). A global differentiation defect should be apparent in genome-wide expression profiles pre-LPS, and a global LPS signaling defect would be apparent post-LPS, while a specific regulatory effect would be manifested as a more specific transcriptional signature.

Pre-LPS (Figure 4B), there were few transcriptional differences between cells in which OSTc is targeted or not (Table S3), except for a group of 60 OST-induced genes that are enriched for the ER stress response (FDR q value = 5.83×10^{-16}, GOrilla). Furthermore, 42 ($p < 10^{-10}$, hypergeometric test) of these genes are bound by the transcription factor XBP1 at their proximal promoter in bone-marrow-derived macrophages (M. Artomov, L. Glimcher, and A.R., unpublished data and Cubillos-Ruiz et al., 2015). Thus, OSTc perturbation has a limited and unique pre-LPS effect on ER stress response genes, and the reduction in CD11c is not associated with a differentiation defect. Notably, N-glycosylation and ER stress were previously shown to interact with the TLR pathway (Komura et al., 2013; Martinon et al., 2010); however, direct involvement of OSTc was not shown.

The LPS response in DCs has been previously characterized (Shalek et al., 2014) by three distinct co-expression signatures: (1) anti-viral genes ("anti-viral"), (2) inflammatory genes, including Tnf, whose expression peaks at 2 hr ("peaked inflammatory"), and (3) inflammatory genes with sustained expression within the 6 hr timescale ("sustained inflammatory"). While several of the mutants in the known TLR pathway genes were defective in activating all three signatures (Figures 5C–5E), targeting OSTc members reduced the inflammatory signatures (sustained: $p = 0.01$; peaked: $p = 0.01$, t test), but not the anti-viral signature ($p = 0.24$, t test) (Figures 4B–4E and 5C–5E), suggesting a specific rather than global effect on the Tlr4 response.

Additional regulators with the same profile as OSTc may regulate Tnf through related pathways. These include *Hsp90b* and *Alg2*, known members of the protein folding and secretion pathways (Figure 4A and Figure S4D) and *Tmem258*, whose human ortholog resides in a locus associated with Crohn's disease (Franke et al., 2010) and targeted by ANRIL, a long non-coding RNA associated with immune and metabolic diseases (Bochenek et al., 2013). Targeting of *Tmem258* induced the same ER stress genes pre-LPS (5/14 genes; 7.7×10^{-5} q-FDR GOrilla; Table S3) and similar profiles post-LPS.

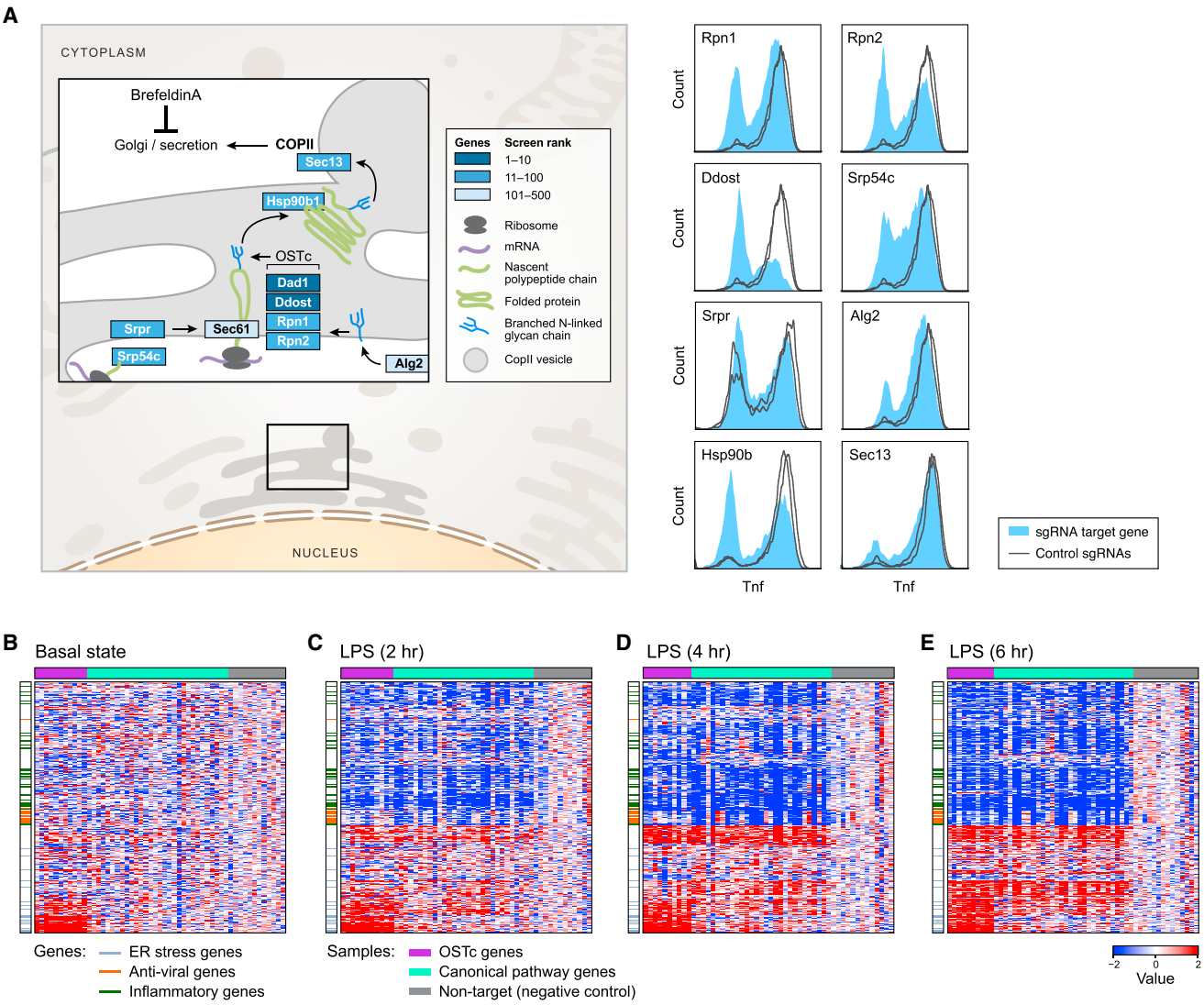

Figure 4. The OST Complex Strongly Affects the BMDC Inflammatory Response

(A) (Left) Positive regulators in the context of the secretory pathway; (right) intracellular Tnf staining for sgRNAs against each targeted gene (filled) versus non-targeting controls (lines).

(B–E) Impact of OSTc perturbation on gene expression at indicated times post LPS. (Heatmaps) Row-normalized Z scores (relative to non-targeting controls) of mRNA levels for each sgRNA-targeted sample (columns). Only mRNAs that are differentially expressed (at least one time point, adjusted $p < 0.001$) are shown, in the same order in each panel.

See also Figure S4.

The PAF Complex and Its Physical Interactors Form a Module that Positively Regulates Tnf Protein Expression

Five of six known subunits of the PAF complex (PAFc; *Paf1*, *Ctr9*, *Wdr61*, *Rtf1*, *Leo1*), a regulator of transcription elongation and 3′ mRNA processing (Jaehning, 2010), were identified as positive regulators of Tnf expression among the top 100 ranked genes in the primary screen; each was validated individually (Figures 3C, 5A, 5B, and S5A), did not significantly affect cell proliferation (data not shown), had a similar effect on RNA and protein expression, and associated most strongly with a single module (Figure 3, blue). The sixth subunit, *Cdc73* (rank 842 in the primary screen), was likely a false negative since two additionally designed sgRNAs did reduce Tnf expression (Figure S5B). The Ash2l subunit of the MLL complex, previously reported to physically interact with Cdc73 (Rozenblatt-Rosen et al., 2005), was also validated as a positive regulator of Tnf in our screen (rank 41, Figure S5B).

Regulation of transcription elongation was previously shown to be an important key step in the DC transcriptional response (Beaudoin and Jaffrin, 1989; Hargreaves et al., 2009). Prior studies have implicated Paf1 or PAFc in regulation of antiviral gene expression (Marazzi et al., 2012), but PAFc was not previously implicated in Tnf or inflammatory gene expression.

To decipher the specific impact of PAFc, we examined its effect on each of the transcriptional signatures. Targeting PAFc

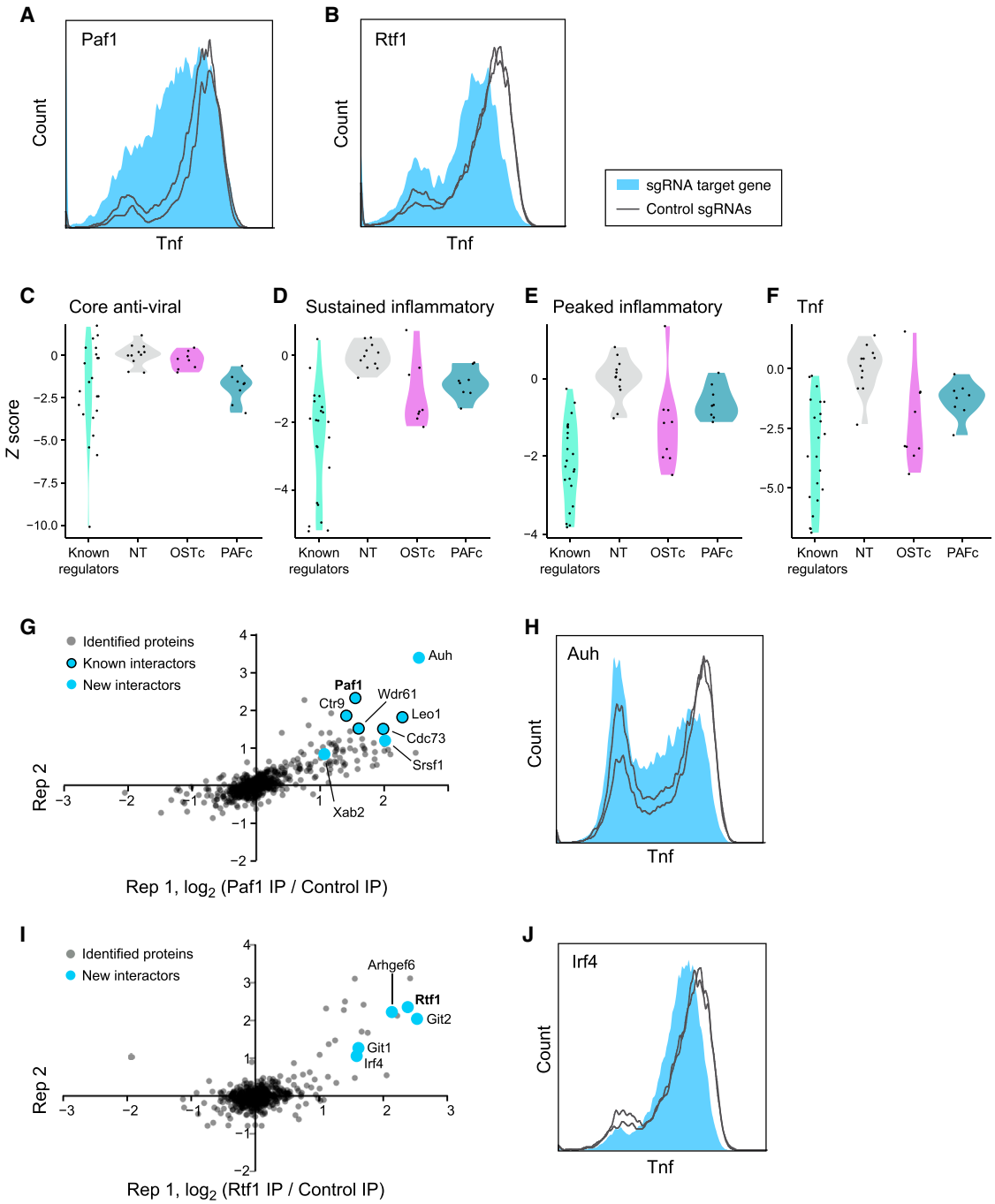

Figure 5. The Paf Complex Strongly Affects the LPS Response

(A and B) Intracellular Tnf staining in cells with sgRNAs targeting Paf1 (A) or Rtf1 (B) (filled), compared to sgRNA controls (lines).

(C–F) Violin plots of the distribution of response scores per sgRNA (calculated as an average of all RNA changes relative to non-targeting controls) in cells treated with sgRNAs targeting known regulators, non-targeting controls (NT), OSTc members, and PAFc members for each of three response signatures: anti-viral (C, 4 hr post-LPS), sustained inflammatory (D, 4 hr post-LPS), and peaked inflammatory (E, 2 hr post-LPS), as well as Tnf transcript (F, 2 hr post-LPS). Positive and negative values: increased and reduced response, respectively.

(G and I) Scatter plots of two independent immunopurifications (IP) of Paf1 (G) or Rtf1 (I) followed by LC-MS/MS. (Blue dots) Interactors tested by individual sgRNA experiments for an effect on Tnf expression. (Bold) IP target.

(H and J) Intracellular Tnf staining in cells with sgRNAs targeting Auh (H) or Irf4 (J) (filled), compared to sgRNA controls (lines).

Also see Figure S5, related to Figure 5.

subunits significantly reduces the expression of the anti-viral and sustained inflammatory signatures (p = 0.0002 and 0.001, respectively, t test) and has a weaker, albeit significant (p = 0.01), effect on the peaked inflammatory signature, including on Tnf mRNA (Figures 5C–5F).

To better understand PAFc's function, we analyzed PAFc interactors by immunopurification of Paf1 from BMDCs followed by mass spectrometry (MS) (Figure 5G and Table S4). We re-identified all known complex components, except Rtf1, and identified interactions with several RNA-processing factors (Table S4), including the AU-rich RNA-binding and leucine metabolism protein AUH (Kurimoto et al., 2009; Nakagawa et al., 1995), an interaction confirmed by western blot (Figure S5E). Using an individual sgRNA targeting *Auh* (Figure 5H), we found significant reductions in Tnf levels, whereas Srsf1 did not affect Tnf levels (Figure S5D). Since AUH binds AU-rich motifs in 3′ UTRs and the stability of the Tnf transcript is known to be regulated through an AU-rich motif by three other RNA-binding proteins (AUF1 [Khabar, 2010], Zfp36 [Carballo et al., 1998], and HuR [Dean et al., 2001; Tiedje et al., 2012]), it would be interesting to test whether AUH also interacts with the 3′ UTR of Tnf directly to regulate RNA levels.

Although Rtf1 interacts with Paf1 in lower organisms (Mueller and Jaehning, 2002), we did not observe a direct interaction between PAFc and Rtf1 when immunopurifying either Paf1 (Figure 5G) or Rtf1 (Figure 5I and Table S4). Of four Rtf1 interactors tested (Git1, Git2, Arhgef6, and Irf4), only one, Irf4, significantly reduced Tnf expression (Figure 5J), consistent with its ranking in the secondary screen (rank 13). We also found that Irf4 affects Cd11c (Figure S5C), consistent with previous findings (Lehtonen et al., 2005; Tussiwand et al., 2012). The interaction between Irf4 and Rtf1 may suggest that PAFc, Rtf1, and other accessory proteins can perform immune-specific transcriptional activation by recruiting sequence-specific transcription factors.

DISCUSSION

We developed a genome-wide genetic screen in primary cells, based on our previous demonstration that the genomes of BMDCs from Cas9-expressing mice could be edited effectively within a relatively short time window ex vivo (Platt et al., 2014). By focusing on a quantitative cellular marker rather than cell viability, we illustrate the versatility of pooled screens and provide an effective approach for screening in primary cells derived from the Cas9 transgenic mouse. Our secondary pooled screen illustrates how increases in the number and efficacy of sgRNAs per gene and number of cells infected per sgRNA can substantially improve the specificity and sensitivity of a pooled screen. We thus employed a strategy that uses the results of the primary screen with a relatively permissive FDR threshold to then guide both a large number of individual sgRNA validation experiments and a secondary screen with a much lower FDR. Using these approaches, we systematically identified previously unrecognized regulators of Tnf in response to LPS, including two conserved protein complexes and many others (e.g., *Tti2*, *Ruvbl2*, *Tmem258*, *Midn*, *Ddx39b*, *Stat5b*, and *Pdcd10*).

To determine whether the genes that affect Tnf act through different cellular pathways, we quantified how these regulators alter expression of additional protein markers and genome-wide mRNAs and partitioned the regulators into three modules that are dominated by known Tlr4 pathway components, the OST complex or the PAF complex (Figure 3), thus providing clues for the functions of genes within each module. While we do not yet have a molecular model for how OSTc and PAFc impact the TLR pathway, we found that targeting subunits of the OSTc results in baseline ER stress that is likely regulated by XBP1 and may contribute to the reduction in TNF response (Cubillos-Ruiz et al., 2015). Our unbiased approach reveals how conserved cellular processes can have relatively specific effects on a well-defined response, offering a more comprehensive and unified view of how cellular functions are linked within a cell.

Our genome-wide, unbiased approach allowed us to uncover new modules and factors even in a heavily investigated immune pathway and will be useful across diverse biological systems, especially when coupled with advances in single-cell profiling that bridge the gap between genome-wide pooled screens and deep molecular readouts.

EXPERIMENTAL PROCEDURES

For full methods see, see the Supplemental Experimental Procedures.

Pooled Genome-wide CRISPR Screens

For the pooled genome-wide CRISPR screen, BMDCs were isolated from 6- to 8-week-old constitutive Cas9-expressing female mice and used as described previously (Platt et al., 2014). Cells were infected with the pooled lentiviral library at an MOI of 1 at day 2. At day 9, BMDCs were stimulated with 100 ng/ml LPS, and after 30 min, Brefeldin A (GolgiPlug, BD Biosciences) was added. After 8 hr of LPS stimulation, cells were harvested, fixed, and stained for Tnf (Ramirez-Ortiz et al., 2015) and Cd11c and then FACS sorted (Supplemental Experimental Procedures). The genome-wide screens were performed as three independent replicates; in the first screen, 60 million infected cells yielded 350 million cells at day 9, while in the second and third screens, 200 million infected cells yielded 1 billion BMDCs at day 9. The secondary pooled screen (using a reduced library) was done using the same protocol with 200 million infected cells. For individual sgRNA experiments, we used a similar protocol, except BMDCs were infected with high MOI and selected with puromycin (Invitrogen).

Cloning of Individual and Libraries of sgRNAs and Subsequent Viral Production

For the primary screen, we used the GeCKOv2mouse library in the lentiGuide-Puro vector (Sanjana et al., 2014). For the secondary screen, we designed 10 sgRNAs per gene (Doench et al., 2014) to target 2,569 of the top genes (Table S5) in the DE analysis of the primary screen and added 2,500 non-targeting sgRNAs (Table S5). For library construction, we used a previously published protocol (Shalem et al., 2014). For individual sgRNA cloning, pairs of oligonucleotides (IDT) with BsmBI-compatible overhangs were separately annealed and cloned into the lentiGuide-Puro plasmid (also available at Addgene, plasmid #52963) using standard protocols. Lentivirus was made using 293T cells transfected with lentiGuide-Puro, psPAX2 (Addgene 12260), and pMD2.G (Addgene 12259) at a 10:10:1 ratio, using Lipofectamine LTX and plus reagents according to the manufacturer's instructions.

Amplification and Sequencing of sgRNAs from Cells

After sorting, DNA was purified using QIAGEN DNeasy Blood & Tissue Kit according to the manufacturer's instruction. PCR was performed as previously described (Shalem et al., 2014), and the PCR products were sequenced on a HiSeq 2500. The reads were aligned to the sgRNAs using Bowtie 1 (Langmead et al., 2009).

Analysis of Screen

To score sgRNAs and genes based on their abundance in the different bins, we used two strategies: in the first (DE), we normalized the raw reads and

averaged on all the sgRNAs per gene and then performed differential expression analysis on three biological repeats using the R package DESeq2 (Love et al., 2014), which fits a negative binomial generalized linear model (GLM). In the second strategy (ZS), we combined all low and high bins from the three experiments into a single pair of TNF^{low} and TNF^{hi} bins, and fold changes of TNF^{low}/TNF^{hi} were Z score normalized. To collapse to gene level, the mean of the top four ranked sgRNAs was taken for positive regulators and the bottom four ranked sgRNAs for negative regulators. For the secondary screen, we used all sgRNAs in both methods. All of the ranks in the paper are based on ZS unless otherwise noted.

Analysis of Protein and RNA Expression

Day 9 differentiated and transduced BMDCs were activated with LPS for 0, 2, 4, and 6 hr for the RNA-seq experiments or for 8 hr before staining with Il-6, MIp1α, CD11c, and CD14 antibody. Cells with gene-specific sgRNAs were compared to those with non-targeting sgRNAs. For RNA purification, we used QIAGEN RNAeasy 96 Kit and constructed RNA libraries using the SMART-seq2 protocol (Picelli et al., 2013) in a 96-well plate format followed by Nextera XT DNA Sample Preparation (Illumina) and deep sequencing on a HiSeq 2500.

Protein Immunopurification

For each IP, 20 million unstimulated BMDCs were used. Each Paf1 or Rtf1 IP was always performed in parallel to a control IP and in two independent replicates. In one replicate of the experiment, the digested proteins were labeled with iTRAQ, and in the second replicate, they were labeled with TMT10plex.

ACCESSION NUMBERS

The RNA-Seq data is deposited in the Gene Expression Omnibus (GEO: GSE67164). The sgRNA sequencing data is deposited in http://www.broadinstitute.org/pubs/TNF_CRISPR_DCs/. The processed mass spectrometry data is reported in Table S4, and raw mass spectrometry data is available upon request.

SUPPLEMENTAL INFORMATION

Supplemental Information includes Supplemental Experimental Procedures, five figures, and five tables and can be found with this article online at http://dx.doi.org/10.1016/j.cell.2015.06.059.

AUTHOR CONTRIBUTIONS

O.P., M.J., T.M.E., N.H., and A.R. conceived and designed the study. O.P., M.J., and T.M.E. conducted the majority of the experiments. In addition, O.P. constructed the sgRNA libraries and performed the RNA-seq experiments, M.J. performed the proteomics experiments together with P.M. and S.A.C., and T.M.E. led the protein staining experiments. R.H.H., A.D., and C.J.Y. performed most of the large-scale data analyses, with help from O.P., R.S., D.P., and I.T. O.S., N.E.S., and F.Z. provided the library, protocols, and guidance in CRISPR screens. R.J.P. and F.Z. generated the Cas9 transgenic mouse. R.R. generated and cultured DCs. O.P., M.J., T.M.E., N.H., and A.R. wrote the manuscript with input from all authors.

ACKNOWLEDGMENTS

We thank Max Artyomov and Laurie Glimcher for help and data related to Xbp1 targets and Jonathan Weissman for very helpful discussions on ER stress. We thank the Broad's Genomic Perturbation Platform for help in design of the secondary library and Broad Technology labs (Tarjei Mikkelssen) for help with synthesis of the secondary library. We thank Dave Gennert, Carl De Boer, Alex Shalek, John Trombetta, Schraga Schwartz, Maxwell Mumbach, Dawn Thompson, Timothy Tickle, Brian Haas, Chloe Villani, and all members of the Regev, Hacohen, Carr, and Zhang groups for input and discussions. We thank Terry Means for discussions and advice. We thank Leslie Gaffney for help with figure preparation and the Broad Genomics Platform for all sequencing. FACS sorting was performed at the Bauer Core Laboratory, Harvard FAS Center for Systems Biology, with great help from Patricia Rogers. This work was supported by NHGRI CEGS P50 HG006193 (A.R., N.H., and S.A.C.) and Broad Institute Funds. A.R. was supported by the Klarman Cell Obervatory and HHMI. N.H. was supported by the MGH Research Scholars Program. M.J. was supported by fellowships of the Swiss National Science Foundation for advanced researchers (SNF) and the Marie Sklodowska-Curie IOF. F.Z. is supported by the National Institutes of Health through NIMH (5DP1-MH100706) and NIDDK (5R01-DK097768), a Waterman Award from the National Science Foundation, the Keck, New York Stem Cell, Damon Runyon, Searle Scholars, Merkin, and Vallee Foundations, and Bob Metcalfe. F.Z. is a New York Stem Cell Foundation Robertson Investigator. N.E.S. is supported by a Simons Center for the Social Brain Postdoctoral Fellowship and NIH NHGRI award K99-HG008171. O.S. is a fellow of the Klarman Cell Observatory. R.J.P. is supported by a National Science Foundation Graduate Research Fellowship under grant number 1122374. I.T. was supported by a Human Frontier Science Program fellowship. A.D. is supported by the National Space Biomedical Research Institute through NASA NCC 9-58 and the National Defense Science and Engineering Fellowship. R.H.H. receives support from the Herchel Smith Fellowship. A.R. is on the scientific advisory board for Thermo Fisher Scientific. F.Z. is a founder and scientific advisor of Editas Medicine and a scientific advisor for Horizon Discovery.

Received: March 1, 2015
Revised: April 25, 2015
Accepted: May 22, 2015
Published: July 16, 2015

REFERENCES

Amit, I., Regev, A., and Hacohen, N. (2011). Strategies to discover regulatory circuits of the mammalian immune system. Nat. Rev. Immunol. *11*, 873–880.

Beaudoin, G., and Jaffrin, M.Y. (1989). Plasma filtration in Couette flow membrane devices. Artif. Organs *13*, 43–51.

Beck, T., Hastings, R.K., Gollapudi, S., Free, R.C., and Brookes, A.J. (2014). GWAS Central: a comprehensive resource for the comparison and interrogation of genome-wide association studies. Eur. J. Hum. Genet. *22*, 949–952.

Bochenek, G., Häsler, R., El Mokhtari, N.E., König, I.R., Loos, B.G., Jepsen, S., Rosenstiel, P., Schreiber, S., and Schaefer, A.S. (2013). The large non-coding RNA ANRIL, which is associated with atherosclerosis, periodontitis and several forms of cancer, regulates ADIPOR1, VAMP3 and C11ORF10. Hum. Mol. Genet. *22*, 4516–4527.

Boehringer, N., Hagens, G., Songeon, F., Isler, P., and Nicod, L.P. (1999). Differential regulation of tumor necrosing factor-alpha (TNF-alpha) and interleukin-10 (IL-10) secretion by protein kinase and phosphatase inhibitors in human alveolar macrophages. Eur. Cytokine Netw. *10*, 211–218.

Carballo, E., Lai, W.S., and Blackshear, P.J. (1998). Feedback inhibition of macrophage tumor necrosis factor-alpha production by tristetraprolin. Science *281*, 1001–1005.

Carette, J.E., Guimaraes, C.P., Varadarajan, M., Park, A.S., Wuethrich, I., Godarova, A., Kotecki, M., Cochran, B.H., Spooner, E., Ploegh, H.L., and Brummelkamp, T.R. (2009). Haploid genetic screens in human cells identify host factors used by pathogens. Science *326*, 1231–1235.

Cubillos-Ruiz, J.R., Silberman, P.C., Rutkowski, M.R., Chopra, S., Perales-Puchalt, A., Song, M., Zhang, S., Bettigole, S.E., Gupta, D., Holcomb, K., et al. (2015). ER stress sensor XBP1 controls anti-tumor immunity by disrupting dendritic cell homeostasis. Cell *161*, 1527–1538.

da Silva Correia, J., and Ulevitch, R.J. (2002). MD-2 and TLR4 N-linked glycosylations are important for a functional lipopolysaccharide receptor. J. Biol. Chem. *277*, 1845–1854.

Darnell, J.E., Jr. (1997). STATs and gene regulation. Science *277*, 1630–1635.

Dean, J.L., Wait, R., Mahtani, K.R., Sully, G., Clark, A.R., and Saklatvala, J. (2001). The 3′ untranslated region of tumor necrosis factor alpha mRNA is a target of the mRNA-stabilizing factor HuR. Mol. Cell. Biol. *21*, 721–730.

Doench, J.G., Hartenian, E., Graham, D.B., Tothova, Z., Hegde, M., Smith, I., Sullender, M., Ebert, B.L., Xavier, R.J., and Root, D.E. (2014). Rational design

of highly active sgRNAs for CRISPR-Cas9-mediated gene inactivation. Nat. Biotechnol. *32*, 1262–1267.

Echeverri, C.J., Beachy, P.A., Baum, B., Boutros, M., Buchholz, F., Chanda, S.K., Downward, J., Ellenberg, J., Fraser, A.G., Hacohen, N., et al. (2006). Minimizing the risk of reporting false positives in large-scale RNAi screens. Nat. Methods *3*, 777–779.

Eden, E., Navon, R., Steinfeld, I., Lipson, D., and Yakhini, Z. (2009). GOrilla: a tool for discovery and visualization of enriched GO terms in ranked gene lists. BMC Bioinformatics *10*, 48.

Faurobert, E., and Albiges-Rizo, C. (2010). Recent insights into cerebral cavernous malformations: a complex jigsaw puzzle under construction. FEBS J. *277*, 1084–1096.

Franke, A., McGovern, D.P., Barrett, J.C., Wang, K., Radford-Smith, G.L., Ahmad, T., Lees, C.W., Balschun, T., Lee, J., Roberts, R., et al. (2010). Genome-wide meta-analysis increases to 71 the number of confirmed Crohn's disease susceptibility loci. Nat. Genet. *42*, 1118–1125.

Gilbert, L.A., Horlbeck, M.A., Adamson, B., Villalta, J.E., Chen, Y., Whitehead, E.H., Guimaraes, C., Panning, B., Ploegh, H.L., Bassik, M.C., et al. (2014). Genome-Scale CRISPR-Mediated Control of Gene Repression and Activation. Cell *159*, 647–661.

Goudreault, M., D'Ambrosio, L.M., Kean, M.J., Mullin, M.J., Larsen, B.G., Sanchez, A., Chaudhry, S., Chen, G.I., Sicheri, F., Nesvizhskii, A.I., et al. (2009). A PP2A phosphatase high density interaction network identifies a novel striatin-interacting phosphatase and kinase complex linked to the cerebral cavernous malformation 3 (CCM3) protein. Mol. Cell. Proteomics *8*, 157–171.

Haeuptle, M.A., and Hennet, T. (2009). Congenital disorders of glycosylation: an update on defects affecting the biosynthesis of dolichol-linked oligosaccharides. Hum. Mutat. *30*, 1628–1641.

Hargreaves, D.C., Horng, T., and Medzhitov, R. (2009). Control of inducible gene expression by signal-dependent transcriptional elongation. Cell *138*, 129–145.

Hart, T., Brown, K.R., Sircoulomb, F., Rottapel, R., and Moffat, J. (2014). Measuring error rates in genomic perturbation screens: gold standards for human functional genomics. Mol. Syst. Biol. *10*, 733.

Huffaker, T.C., and Robbins, P.W. (1983). Yeast mutants deficient in protein glycosylation. Proc. Natl. Acad. Sci. USA *80*, 7466–7470.

Jaehning, J.A. (2010). The Paf1 complex: platform or player in RNA polymerase II transcription? Biochim. Biophys. Acta *1799*, 379–388.

Kanehisa, M., and Goto, S. (2000). KEGG: kyoto encyclopedia of genes and genomes. Nucleic Acids Res. *28*, 27–30.

Khabar, K.S. (2010). Post-transcriptional control during chronic inflammation and cancer: a focus on AU-rich elements. Cell. Mol. Life Sci. *67*, 2937–2955.

Kim, H.D., Shay, T., O'Shea, E.K., and Regev, A. (2009). Transcriptional regulatory circuits: predicting numbers from alphabets. Science *325*, 429–432.

Koesters, C., Unger, B., Bilic, I., Schmidt, U., Bluml, S., Lichtenberger, B., Schreiber, M., Stockl, J., and Ellmeier, W. (2007). Regulation of dendritic cell differentiation and subset distribution by the zinc finger protein CTCF. Immunol. Lett. *109*, 165–174.

Komura, T., Sakai, Y., Honda, M., Takamura, T., Wada, T., and Kaneko, S. (2013). ER stress induced impaired TLR signaling and macrophage differentiation of human monocytes. Cell. Immunol. *282*, 44–52.

Konermann, S., Brigham, M.D., Trevino, A.E., Joung, J., Abudayyeh, O.O., Barcena, C., Hsu, P.D., Habib, N., Gootenberg, J.S., Nishimasu, H., et al. (2015). Genome-scale transcriptional activation by an engineered CRISPR-Cas9 complex. Nature *517*, 583–588.

Kurimoto, K., Kuwasako, K., Sandercock, A.M., Unzai, S., Robinson, C.V., Muto, Y., and Yokoyama, S. (2009). AU-rich RNA-binding induces changes in the quaternary structure of AUH. Proteins *75*, 360–372.

Langmead, B., Trapnell, C., Pop, M., and Salzberg, S.L. (2009). Ultrafast and memory-efficient alignment of short DNA sequences to the human genome. Genome Biol. *10*, R25.

Lehtonen, A., Veckman, V., Nikula, T., Lahesmaa, R., Kinnunen, L., Matikainen, S., and Julkunen, I. (2005). Differential expression of IFN regulatory factor 4 gene in human monocyte-derived dendritic cells and macrophages. J. Immunol. *175*, 6570–6579.

Love, M.I., Huber, W., and Anders, S. (2014). Moderated estimation of fold change and dispersion for RNA-seq data with DESeq2. Genome Biol. *15*, 550.

Marazzi, I., Ho, J.S., Kim, J., Manicassamy, B., Dewell, S., Albrecht, R.A., Seibert, C.W., Schaefer, U., Jeffrey, K.L., Prinjha, R.K., et al. (2012). Suppression of the antiviral response by an influenza histone mimic. Nature *483*, 428–433.

Martinon, F., Chen, X., Lee, A.H., and Glimcher, L.H. (2010). TLR activation of the transcription factor XBP1 regulates innate immune responses in macrophages. Nat. Immunol. *11*, 411–418.

Mueller, C.L., and Jaehning, J.A. (2002). Ctr9, Rtf1, and Leo1 are components of the Paf1/RNA polymerase II complex. Mol. Cell. Biol. *22*, 1971–1980.

Nakagawa, J., Waldner, H., Meyer-Monard, S., Hofsteenge, J., Jenö, P., and Moroni, C. (1995). AUH, a gene encoding an AU-specific RNA binding protein with intrinsic enoyl-CoA hydratase activity. Proc. Natl. Acad. Sci. USA *92*, 2051–2055.

Nikolic, T., Movita, D., Lambers, M.E., Ribeiro de Almeida, C., Biesta, P., Kreefft, K., de Bruijn, M.J., Bergen, I., Galjart, N., Boonstra, A., and Hendriks, R. (2014). The DNA-binding factor Ctcf critically controls gene expression in macrophages. Cell. Mol. Immunol. *11*, 58–70.

Picelli, S., Björklund, A.K., Faridani, O.R., Sagasser, S., Winberg, G., and Sandberg, R. (2013). Smart-seq2 for sensitive full-length transcriptome profiling in single cells. Nat. Methods *10*, 1096–1098.

Platt, R.J., Chen, S., Zhou, Y., Yim, M.J., Swiech, L., Kempton, H.R., Dahlman, J.E., Parnas, O., Eisenhaure, T.M., Jovanovic, M., et al. (2014). CRISPR-Cas9 knockin mice for genome editing and cancer modeling. Cell *159*, 440–455.

Ramirez-Ortiz, Z.G., Prasad, A., Griffith, J.W., Pendergraft, W.F., 3rd, Cowley, G.S., Root, D.E., Tai, M., Luster, A.D., El Khoury, J., Hacohen, N., and Means, T.K. (2015). The receptor TREML4 amplifies TLR7-mediated signaling during antiviral responses and autoimmunity. Nat. Immunol. *16*, 495–504.

Rozenblatt-Rosen, O., Hughes, C.M., Nannepaga, S.J., Shanmugam, K.S., Copeland, T.D., Guszczynski, T., Resau, J.H., and Meyerson, M. (2005). The parafibromin tumor suppressor protein is part of a human Paf1 complex. Mol. Cell. Biol. *25*, 612–620.

Sanjana, N.E., Shalem, O., and Zhang, F. (2014). Improved vectors and genome-wide libraries for CRISPR screening. Nat. Methods *11*, 783–784.

Sebastián, C., Serra, M., Yeramian, A., Serrat, N., Lloberas, J., and Celada, A. (2008). Deacetylase activity is required for STAT5-dependent GM-CSF functional activity in macrophages and differentiation to dendritic cells. J. Immunol. *180*, 5898–5906.

Shalek, A.K., Satija, R., Shuga, J., Trombetta, J.J., Gennert, D., Lu, D., Chen, P., Gertner, R.S., Gaublomme, J.T., Yosef, N., et al. (2014). Single-cell RNA-seq reveals dynamic paracrine control of cellular variation. Nature *510*, 363–369.

Shalem, O., Sanjana, N.E., Hartenian, E., Shi, X., Scott, D.A., Mikkelsen, T.S., Heckl, D., Ebert, B.L., Root, D.E., Doench, J.G., and Zhang, F. (2014). Genome-scale CRISPR-Cas9 knockout screening in human cells. Science *343*, 84–87.

Tiedje, C., Ronkina, N., Tehrani, M., Dhamija, S., Laass, K., Holtmann, H., Kotlyarov, A., and Gaestel, M. (2012). The p38/MK2-driven exchange between tristetraprolin and HuR regulates AU-rich element-dependent translation. PLoS Genet. *8*, e1002977.

Tussiwand, R., Lee, W.L., Murphy, T.L., Mashayekhi, M., Kc, W., Albring, J.C., Satpathy, A.T., Rotondo, J.A., Edelson, B.T., Kretzer, N.M., et al. (2012). Compensatory dendritic cell development mediated by BATF-IRF interactions. Nature *490*, 502–507.

Wang, T., Wei, J.J., Sabatini, D.M., and Lander, E.S. (2014). Genetic screens in human cells using the CRISPR-Cas9 system. Science *343*, 80–84.

Yamashita, N., Shimazaki, N., Ibe, S., Kaneko, R., Tanabe, A., Toyomoto, T., Fujita, K., Hasegawa, T., Toji, S., Tamai, K., et al. (2001). Terminal deoxynucleotidyltransferase directly interacts with a novel nuclear protein that is homologous to p65. Genes Cells *6*, 641–652.

Zielinska, D.F., Gnad, F., Wiśniewski, J.R., and Mann, M. (2010). Precision mapping of an in vivo N-glycoproteome reveals rigid topological and sequence constraints. Cell *141*, 897–907.

Cell

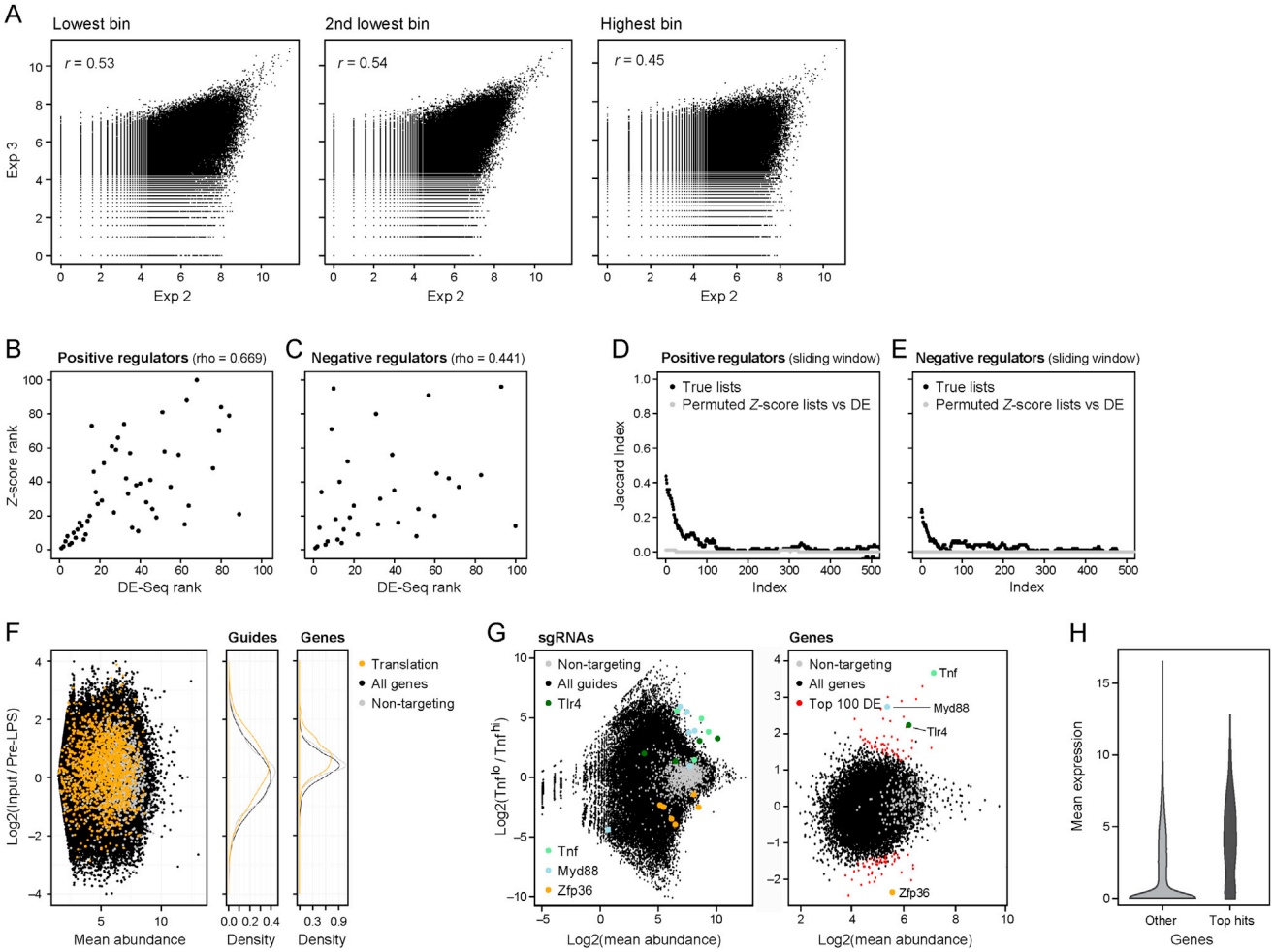

Figure S1. Quality Measures of a Genome-wide Pooled CRISPR Screen in Mouse Primary DC, Related to Figure 1

(A) Reproducibility. Shown are scatterplots comparing the $\log_2$(quantile normalized read counts) of sgRNAs between two replicate screens for the lowest bin (left), 2nd lowest bin (middle), and highest bin (right). Pearson correlation coefficient (*r*) is shown in top left corner. (B-E) Top ranked screen hits compare well between the DESeq and Z-score approaches. (B,C) Scatter plots compare the ranks based on the DE-Seq approach (x axis) and Z score approach (y axis) for either positive regulators (B) or negative regulators (C) among the top-100 ranked genes. The Spearman rank correlation coefficient (ρ) is noted. (D, E) Shown is the Jaccard index between the Z-score and DE-Seq based approaches (y axis, intersection over union) for sliding windows of 50 genes from top of the ranked lists (x axis) for the true ranking (black) and with random shuffling (gray) of the Z-score ranks, for either the positive (D) or negative (E) regulators. The signal is diminished at rank ~150 and ~50 for positive and negative regulators, respectively. (F) sgRNAs that target translation genes are enriched in the "Input" library versus "Pre-LPS." Left: Scatterplot compares the normalized fold change in sgRNAs (Input / Pre-LPS) to the mean abundance in the two libraries. Middle and Right: Distribution of the normalized fold change (Input / Pre-LPS; y axis) in either sgRNAs (middle) or genes (right; mean of the top 4 ranked sgRNAs). Orange: translation genes; black: all genes; gray: non-targeting controls. (G) sgRNAs targeting known regulators of LPS response are highly significant in DE-Seq analysis. MA-plots compare for either sgRNAs (left) or genes (right), the DE-Seq calculated fold-change between TNF^{hi} and TNF^{low} (y axis) to the mean abundance of the sgRNA or gene. (H) Screen hits are more likely to be expressed post-LPS and at higher level than all other genes. Violin plots show the distribution of mean expression (y axis) along LPS stimulation (0h, 2h, 4h, 6h) in control cells, for top-169 hits (right) and for all other genes (left).

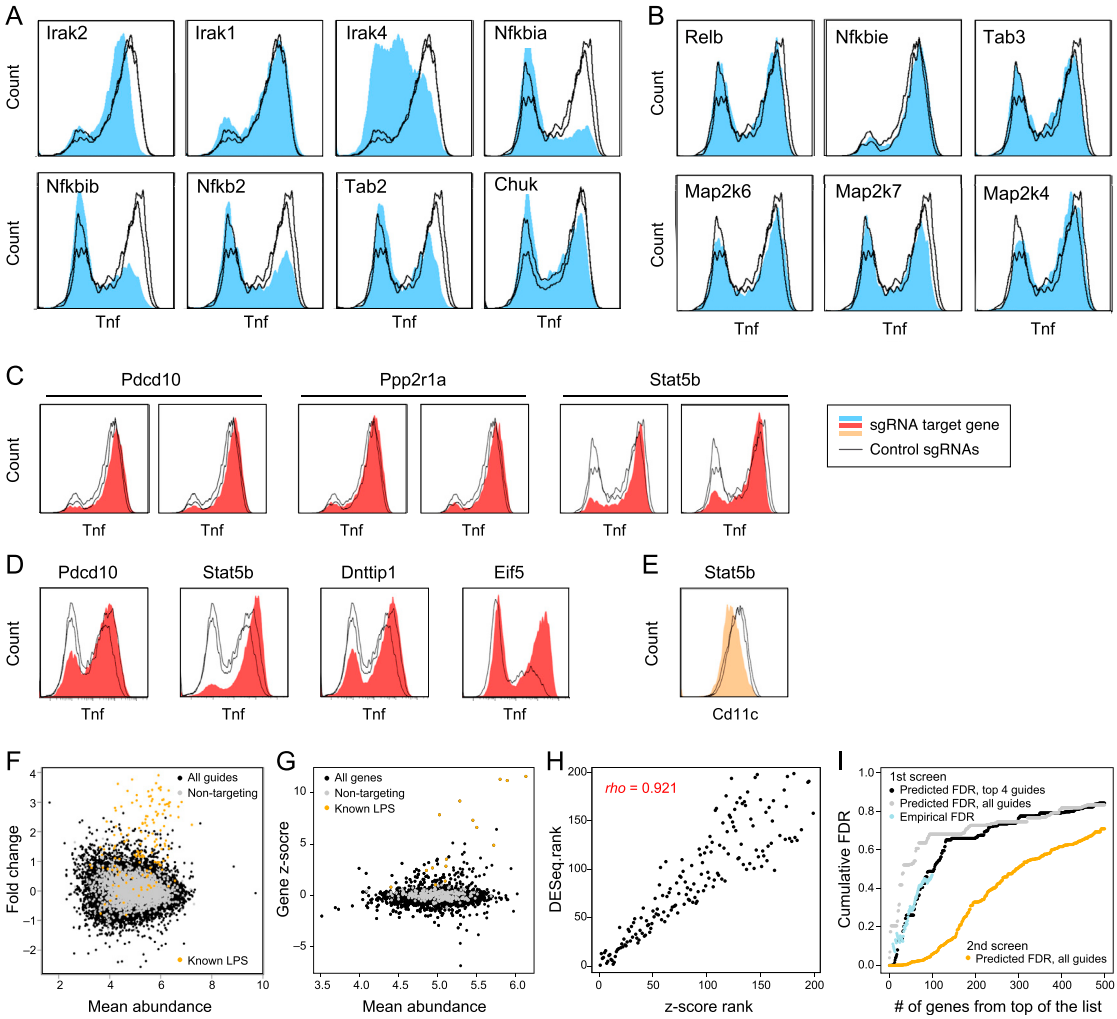

Figure S2. Assessing False Negatives, Negative Regulators, and Analysis of the Secondary Library, Related to Figure 2

Each panel in A-D shows flow cytometry staining of intracellular Tnf levels (x axis) for each targeted gene (colored histogram; gene name in top left corner) compared to sgRNA controls (black curves). (A, B) Determining the false negative rate. Known regulators of the LPS response that did not rank within the top-100 in the screen were tested individually by single sgRNAs followed by Tnf staining and flow cytometry (Figure 2A). (A) 8 tested genes did influence Tnf expression and are considered false negatives. (B) 6 tested genes did not influence Tnf expression and are considered true negatives. (C-E) Sensitive validation of novel negative regulators requires screening at unsaturated levels of Tnf. BMDCs transduced with single sgRNAs targeting candidate negative regulators from the screen, and stained with anti-Tnf antibody after stimulation with either (C) 100ng/mL LPS (two different sgRNAs shown for each gene) or (D) 20ng/mL LPS (single sgRNA shown for each gene). (E) BMDCs transduced with an sgRNA targeting Stat5b were stained with Cd11c antibody. (F-G) Secondary library sgRNAs targeting known regulators of LPS response (orange) have highly significant Z-scores, compared to those targeting other genes (black) and non-targeting controls (gray). Shown are MA-plots that relate for either sgRNAs (F) or genes (G) the fold-change or z-score, respectively, between TNF^{hi} and TNF^{low} (y axis) to the mean abundance of the sgRNA or gene (x axis). (H) Top ranked screen hits compare well between the DE and ZS approaches. Scatter plot compares the ranks of each gene by the DE (y axis) and ZS (x axis) approaches, for the top ranked 200 genes, of which they share 170. The Spearman rank correlation coefficient is noted at the upper left corner. (I) Secondary screen improves specificity. Shown are the theoretically estimated FDRs (y axis), based on shuffling the guides before collapsing to genes, for the secondary screen (orange) and the primary screen (calculated as elsewhere based on top 4 sgRNAs, black; or according to all sgRNAs, gray). The empirical FDR for the first screen, as determined by validation experiments, is marked by light blue at all ranks up to 100.

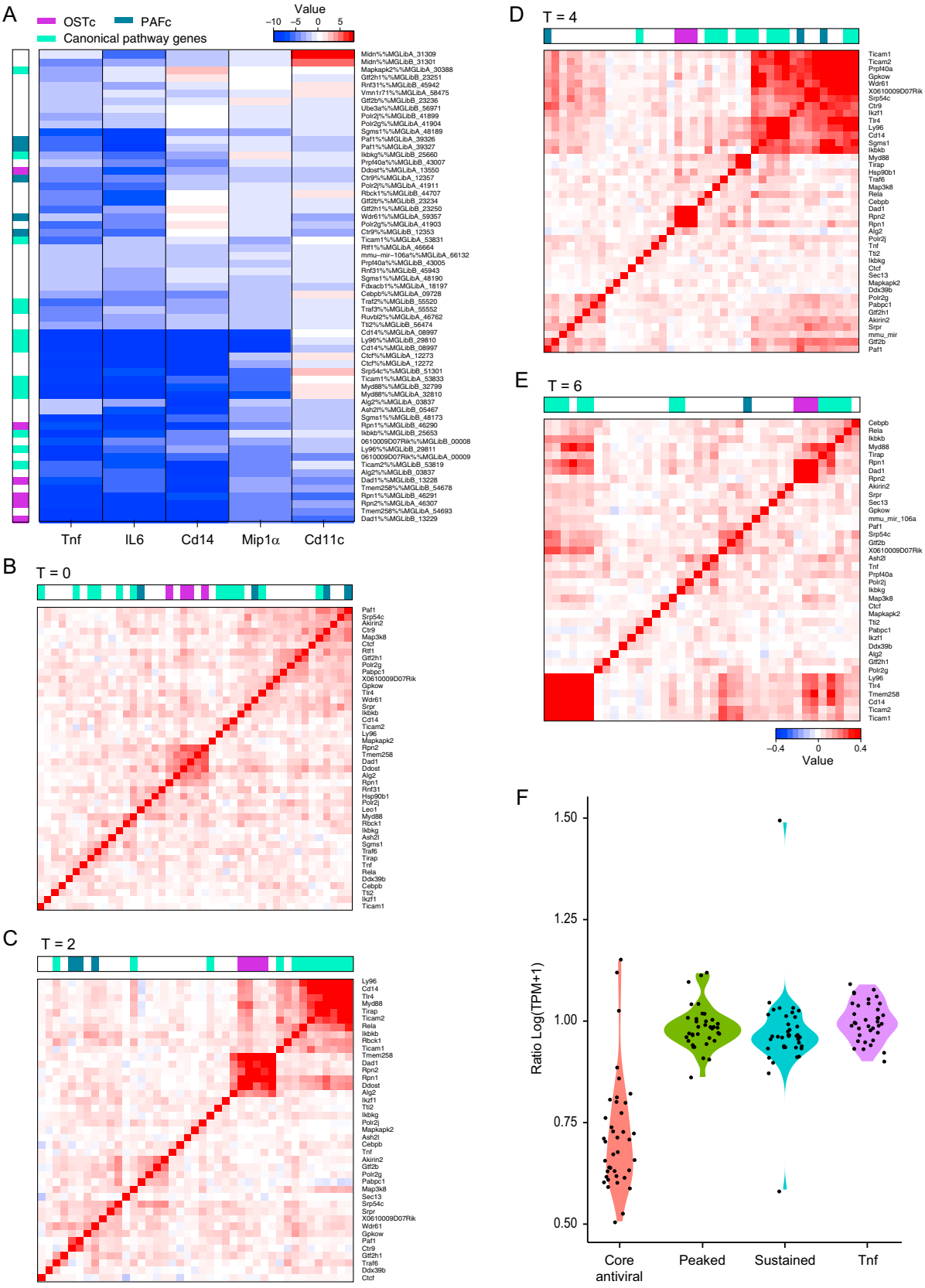

(legend on next page)

Figure S3. Partitioning of the Validated Positive Regulators into Key Modules by Their Effect on Protein Markers and RNA Profiles and the Effect of Brefeldin A, Related to Figure 3

(A) Positive regulators group by distinct effects on protein expression. For each sgRNA targeting a positive regulator (rows) shown are its effects (Z score for each marker compared to non-target sgRNA; Experimental Procedures) on the expression of each of five proteins (columns) measured by staining with antibodies (Experimental Procedures). Three broad categories of responses can be defined, each preferentially associated with distinct proteins. Based on this matrix, sgRNAs were collapsed to score gene level effects as in Figure 3A. (B-E) Positive regulators partition to modules based on their effect on mRNA profiles over time. Shown are clustered correlation matrix of verified positive regulators (rows, columns) based on global RNA expression profiles in cells where the regulator is targeted relative to non-targeting control (Experimental Procedures). Data from each time point is analyzed and clustered (B) t = 0h; (C) t = 2h; (D) t = 4h; (E) t = 6h). Genes in 3 key categories are color coded as in (A). Color bar is the Pearson correlation coefficient. Matrices are exactly as shown in Figure 3D-F, except that a matrix is also shown for t = 6h, and that gene names are labeled. (F) Effect of Brefeldin on the expression of the different modules. Violin plots show for each validated regulator (dot) the ratio of expression values (log(TPM+)) when comparing between Brefeldin versus no Brefeldin conditions, in each of 3 modules and TNF (x axis).

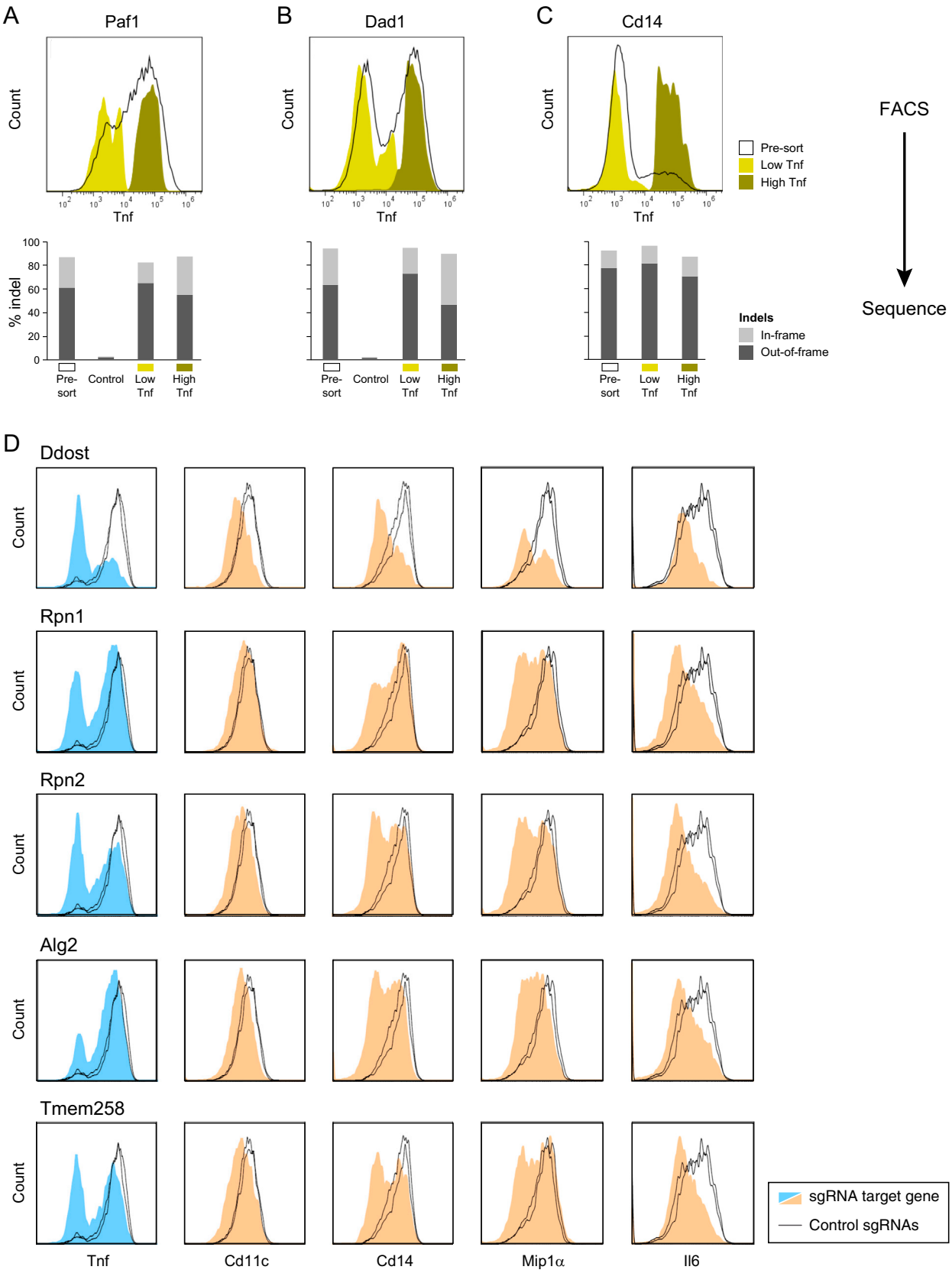

(legend on next page)

Figure S4. Sequence Analysis of Sorted Mutants and the Effect of Knockout OSTc Subunits on Different Markers, Related to Figure 4

BMDCs were transduced with sgRNA targeting the indicated gene ((A) Paf1, (B) Dad1 and (C) Cd14; marked on top), stimulated with LPS, and flow-sorted based on high or low Tnf antibody staining. Genomic DNA was isolated from sorted cells ("low Tnf" and "high Tnf"), unsorted cells ("Pre-sort"), and cells without relevant sgRNA (control; only in A and C). The region surrounding the sgRNA target site was amplified and sequenced to analyze mutational composition of the targeted locus. (D) Each panel shows flow cytometry staining of the levels (x axis) of each of five protein markers (from left to right: Tnf, Cd11c, Cd14, Mip1α, Il6) in cells with individual sgRNA targeting specific genes (colored histogram; gene name on top) compared to sgRNA controls (black curves). Data is shown (from top to bottom) for three representative members of OSTc (Ddost, Rpn1, Rpn2), and two other members of the module: Alg2 and Tmem258.

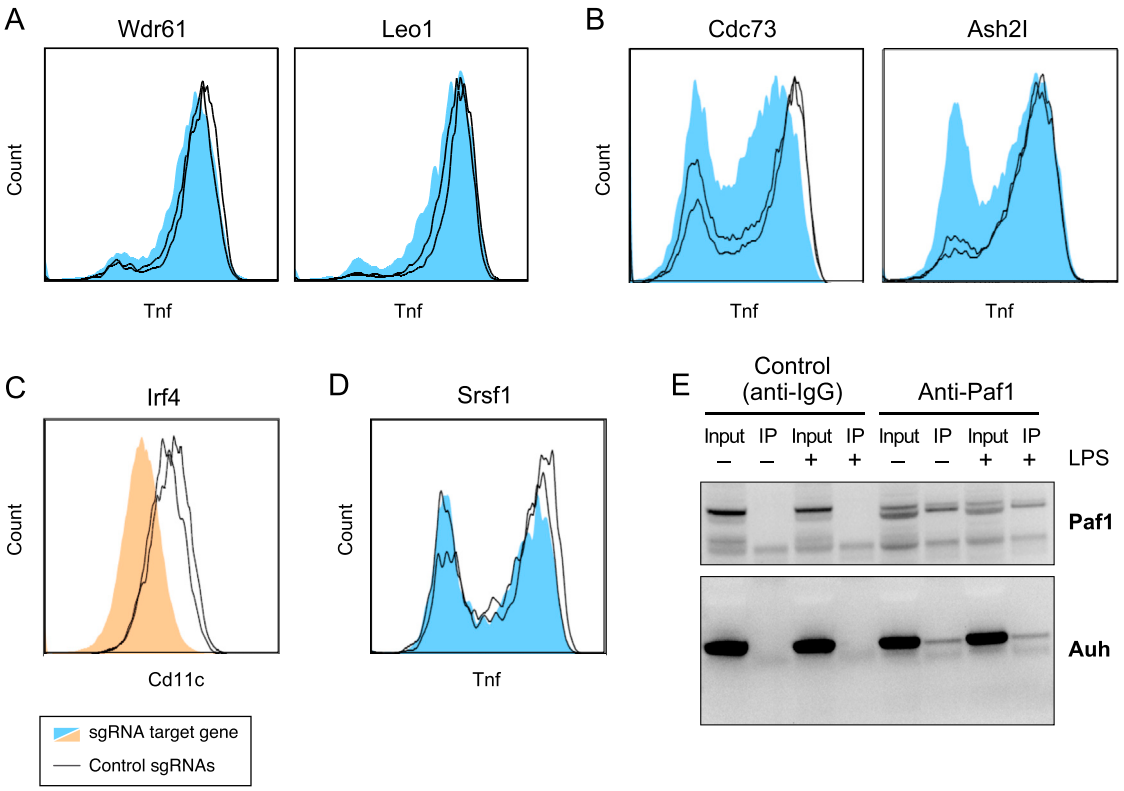

Figure S5. The PAFc Module, Related to Figure 5

(A-D) Each panel shows flow cytometry staining of either intracellular Tnf levels (A, B, D; x axis) or Cd11c levels (C, x axis) for each targeted gene (colored histogram; gene name in top left corner) compared to sgRNA controls (black curves). (E) Validation of Paf1 and Auh interaction by western blot. Shown are the immunopurifications (IPs) in BMDCs performed with either Paf1 antibody (PAF) or IgG antibody (Control). Input or IP samples were incubated with either Paf1 antibody (top) or Auh antibody (bottom). IPs were performed in unstimulated BMDCs (LPS "-") or in BMDCs stimulated with LPS for 2h (LPS "+ ").

Cell

Supplemental Information

A Genome-wide CRISPR Screen in Primary Immune Cells to Dissect Regulatory Networks

Oren Parnas, Marko Jovanovic, Thomas M. Eisenhaure, Rebecca H. Herbst, Atray Dixit, Chun Jimmie Ye, Dariusz Przybylski, Randall J. Platt, Itay Tirosh,Neville E. Sanjana, Ophir Shalem, Rahul Satija, Raktima Raychowdhury, Philipp Mertins, Steven A. Carr, Feng Zhang, Nir Hacohen, and Aviv Regev

Supplemental Experimental Procedures

Bone marrow derived dendritic cells (BMDCs)

All animal protocols were reviewed and approved by the MIT / Whitehead Institute / Broad Institute Committee on Animal Care (CAC protocol 0609-058-12). To obtain sufficient number of cells, we implemented a modified version of the DCs isolation protocol as previously described (Amit et al., 2009; Chevrier et al., 2011; Garber et al., 2012; Lutz et al., 1999). Briefly, for all CRISPR knockout experiments six- to eight-week old constitutive Cas9-expressing female mice were used as described previously (Platt et al., 2014). For all other experiments C57BL/6J female mice were obtained from the Jackson Laboratories. RPMI medium (Invitrogen) supplemented with 10% heat inactivated FBS (Invitrogen), β-mercaptoethanol (50μM, Invitrogen), L-glutamine (2mM, VWR), penicillin/streptomycin (100U/ml, VWR), MEM non-essential amino acids (1X, VWR), HEPES (10mM, VWR), sodium pyruvate (1mM, VWR), and GM-CSF (20 ng/ml; Peprotech) was used throughout the study.

Primary and Secondary Screen

At day 0, cells were collected from femora and tibiae and plated in 100mm non tissue culture treated plastic dishes using 10ml medium per plate at concentration of 2×10^5/ml. At day 2, cells were infected with the pooled lentiviral library at an MOI of 1 and 6 hours later fed with another 10ml of medium per dish. At day 5, 12ml of the medium were carefully removed (to avoid removal of cells) and 10ml of fresh medium were added back to the original dish. Cells were fed with another 5ml medium at day 7. At day 8, all non-

adherent and loosely bound cells were collected and harvested by centrifugation. Cells were then re-suspended with medium, plated at a concentration of $10x10^6$ cells in 10ml medium per 100mm dish. At day 9, cells were stimulated for various time points with LPS (100ng/ml, rough, ultrapure *E. coli* K12 strain, Invitrogen) and harvested.

For the primary screen we sorted the cells as shown in **Figure 1B**, each of the three bins containing approximately 5% of the cells. For the secondary screen, we sorted the cells to two bins: low (15%) and high (5%). The sorted cells in the low bin were divided to three samples and the libraries were prepared separately.

Volumes were adjusted in proportion for different sized plates or wells (e.g. 96 well plates), but cells were always plated at concentration of 2×10^5/ml at day 0.

Individual sgRNA CRISPR knockout experiments

Individual sgRNA mediated CRISPR knockout experiments were performed as described previously (Platt et al., 2014). Briefly, BMDCs were isolated and grown as described above, but in addition were infected with lentiviruses encoding sgRNAs of interest at high MOI at day 2. Cells were expanded in the presence of GM-CSF. At day 6, infected cells were selected by adding puromycin (Invitrogen) at 5 μg/ml. At day 9, cells were stimulated with LPS for the appropriate time and harvested. For subsequent antibody staining (*e.g.*, anti-Tnf), cells were stimulated with 100 ng/ml LPS (or 20 ng/ml for a number of potential negative regulators; see **Results**) and after 30min Brefeldin A (GolgiPlug™, BD Biosciences) was added to trap secreted protein within the cells. 8h post LPS stimulation the cells were harvested, fixed and stained.

Virus production

To produce lentivirus for the screen, we used the GeCKOv2mouse library in the lentiGuide-Puro vector (Sanjana et al., 2014). 10cm plates of 70% confluent 293T cells were transfected with 9 μg of the plasmid library, 9 μg of PAX2 vector (Addgene) and 0.9 μg pVSVg using Lipofectamine® LTX and plus reagents according to the manufacturer's instructions. Supernatant was collected after 48 and 72 hours and then spun for 10 min at 4°C (3000 RPM) and then filtered with a 0.45μm membrane (PALL) and concentrated using Millipore® Amicon® Ultra-15 Centifugal Filter (40 min at 4°C at 4000 RPM). The virus was aliquoted and frozen at -80°C. The titer of the virus was determined by using BMDC from C57BL/6 mice followed by puromycin selection.

To produce lentiviruses containing individual sgRNAs for all validation and follow-up experiments, we used 96 well plates, analogous to the way described above, but with 1% of the reagents, without filtering or concentrating the virus. 20μl of the virus was then used to infect cells in each well of a 96 well plate and 200 μl to infect cells in each well in 12 well plates (in both cases the BMDCs were derived from Cas9 expressing mice).

Fluorescent cell staining and FACS

For the pooled genome-wide and secondary CRISPR screens, BMDC activated with LPS in the presence of Brefeldin A were harvested on ice by scraping, washed twice with cold PBS, and fixed in 4% formaldehyde (Thermo Scientific) for 10 minutes at room temperature. After a further PBS wash, cells were washed with PBS containing 0.1% saponin (Sigma) and resuspended in PBS containing 0.1% saponin supplemented with the

following fluorescent antibodies: eBioscience 12-7321-81 Anti-Mouse TNF alpha PE, Biolegend 117309 APC anti-mouse CD11c Antibody diluted 1:200. After an incubation of 30 minutes on ice, the stained cells were washed once with PBS containing 0.1% saponin, and twice with PBS before sorting.

FACS sorting was performed at the Bauer Core Laboratory, Harvard FAS Center for Systems Biology, Cambridge, MA. In two out of the three replicates of the screen, Cd11c+ cells were sorted into three bins. Two bins had low Tnf expression, to capture cells containing sgRNA targeting positive regulators. The third bin collected the highest 5% of Tnf-expressing cells. In the first experiment, the cells were sorted into two bins (low and high). The bin boundaries were guided by our observations of Tnf expression in cells infected with sgRNAs targeting the known regulators Tlr4, Myd88, and Zfp36 (**Figure 1A**).

For non-pooled CRISPR knockout experiments with individual sgRNAs, cell harvesting and staining was as described above, with the following modifications. Because of cell death caused by puromycin selection of lentivirus-infected cells, dead cells were labeled prior to fixation with Fixable Viability Dye eFluor® 520 (eBioscience) in the majority of experiments, following the manufacturer's instructions. In these experiments, each sample was divided in half after fixation and stained with two antibody panels. Both panels contained Biolegend 117326 PerCP anti-mouse CD11c Antibody. Panel 1 additionally contained Tnf-PE as described above and eBioscience 17-0141-81 Anti-Mouse CD14 APC. Panel 2 additionally contained R&D Systems IC450P Mouse

CCL3/MIP-1 alpha Phycoerythrin mAb, and Biolegend 504508 APC anti-mouse IL-6 Antibody. In a minority of experiments, cells were stained with only one panel, in the same way as for the screen, with the addition of eBioscience 11-0141-82 Anti-Mouse CD14 FITC. All antibody dilutions were 1:200, except anti-CCL3/Mip-1 alpha was 1:20. Flow cytometry was performed on a BD Accuri C6 cytometer in 96- well plates. Analysis was done with FlowJo (Treestar).

In non-pooled CRISPR knockout experiments with individual sgRNAs, low cell growth or viability could be caused by sgRNA-mediated mechanisms, or by low lentiviral titer. To distinguish between these, we separately transduced BMDC from Cas9 mice and C57BL/6 mice (which do not express Cas9). On day 9 of cell growth we harvested the cells and measured viability with Fixable Viability Dye eFluor® 520 followed by flow cytometry analysis, as described above. An sgRNA was considered to cause a cell growth or viability phenotype if the proportion of live cells in Cas9-expressing cells was reduced compared to the proportion of live cells in the C57BL/6 cells. Based on these experiments, we excluded several genes that reduce viability as well as any guides that did not show a consistent phenotype (**Table S2**).

DNA purification from infected cells and library preparation to determine which sgRNAs were expressed in the infected DCs

DNA was purified using Qiagen DNeasy Blood & Tissue Kit according to the manufacturer's instruction. Briefly, the cross-linked cells were first treated with

Proteinase K and incubated at 55°C for 4h to de-crosslink the DNA. DNA was purified according to the kit's protocol and eluted in 400 μl H_2O. We performed two successive PCR reactions of 20 cycles each as described previously (Shalem et al., 2014) using Herculase II Fusion DNA Polymerase (Agilent). 15μl from the first PCR was used for the second PCR (100μl) primers included barcodes as described (Shalem et al., 2014). The final PCR product was run on a gel and the right size fragment was gel extracted and sequenced on a Hi-seq 2500. On average, we sequenced 4-6 aligned reads per sorted cell in each of the bins.

Cloning individual sgRNAs

Pairs of oligonucleotides (IDT) with BsmBI-compatible overhangs were separately annealed and ligated to lentiGuide-Puro plasmid (also available at Addgene, plasmid # 52963) using standard protocols. sgRNA target sequences were taken from the GeCKO library (Sanjana et al., 2014) to validate screen results, or were generated using a previously described sgRNA design algorithm (Doench et al., 2014) (**Table S5**).
Oligonucleotide pairs were designed as follows:
Forward: 5' CACCG<sgRNA target sequence> 3'
Reverse: 5' AAAC<sgRNA target reverse complement>C 3'

In addition, for the initial calibration experiment (**Figure 1A**) we used the following sgRNAs:
Myd88 5' CCCACGTTAAGCGCGACCAA 3'
Zfp36%%MGLibA_60687 5' GGATCTCTCTGCCATCTACG 3'

Tlr4%%MGLibA_54042 5’ GATCTACTCGAGTCAGAATG 3’

NonTargeting 5’ GGGGTAGGCCTAATTACGGA 3’

Design and cloning of the secondary library

For the secondary screen, we targeted the top 2,569 genes in the DE analysis of the primary screen. We used the method of (Doench et al., 2014) to design 10 sgRNAs per gene and included another 2,500 non targeting sgRNAs (**Table S5**). For library construction we used a previously published protocol (Shalem et al., 2014). Briefly, synthesized oligos (Broad Technology Labs) were amplified using the following primers:

Forward

TAACTTGAAAGTATTTCGATTTCTTGGCTTTATATATCTTGTGGAAAGGAC

GAAACACCG

Reverse ACTTTTTCAAGTTGATAACGGACTAGCCTTATTTTAACTTGCTATTTCT

AGCTCTAAAAC

and cloned to BsmBI (Fermentas) digested lentiGuide-Puro plasmid (also available at Addgene, plasmid # 52963) using Gibson ligation reaction (NEB). The ligation reaction was performed using molar ratio of 1:5 of the vector to insert.

Electrocompetent Endura™ Competent Cells (Lucigen) were transformed with the products of the ligation reaction according to the manufacturer’s protocol using a GenePulser (BioRad). 10 parallel transformations were performed and plated onto 245 mm x 245 mm plates with carbenicillin selection (100 ug/ml), for 16 hours at 32 degrees. Colonies were collected and plasmid DNA extraction was made using Endotoxin-Free

Plasmid Maxiprep (Qiagen). Virus production and all subsequent steps were performed as described for the primary screen.

sgRNA sequence analysis

Raw sequencing reads were converted to FASTA files using fastq_to_fasta (FASTX-Toolkit http://hannonlab.cshl.edu/fastx_toolkit/), sequences flanking the guides sequence were trimmed using cutadapt-1.4.1 (Martin 2011) and the trimmed reads were aligned to the sgRNA sequences in the plasmid library using Bowtie 1 (Langmead et al., 2009), with no mismatches allowed. To exclude lowly abundant sgRNAs, the lowest 5% quantile of guides in the input lentiviral libraries was removed from all samples.
In the last two replicate experiments of the screen, we found sgRNA contamination that resulted from individual sgRNA cloning of the following guides: Tlr4%%MGLibA_54042, Tlr4%%MGLibB_54025, Dgke%%MGLibB_14010, Dgke%%MGLibA_14019, Rab13%%MGLibB_44085, Rab13%%MGLibA_44099, Tnf%%MGLibB_55164, Tnf%%MGLibA_55183. Those guides were discarded from our analysis.

Since the C57BL/6 genome was the template for the sgRNA, we assessed the possibility that any sgRNA overlapped a single nucleotide polymorphism (SNP) in two additional genomes that contributed to the CAS-9 transgenic mice. Specifically, The CAS-9 mice were created using 3 different mouse strains, C57BL/6, 129 and FVB. In order to examine possible effects of single nucleotide polymorphism (SNP) between the strains on the sgRNA efficiency, we compared the coordinates of the SNP data

(http://www.sanger.ac.uk/resources/mouse/genomes/) to the genomic mappings of the sgRNA sequences. Of 119,364 sgRNA sequences perfectly and uniquely matching the mm10 genome, only 3,350 sgRNA contained one SNP to one of the other two genomes, 255 sgRNAs contained 2 SNPs and 34 sgRNAs contained 3 or more SNPs.

Scoring sgRNA enrichment or depletion by differential expression analysis

To score sgRNAs whose levels are distinct between the TNF^{low} and TNF^{hi} cells, we used a differential expression analysis. First, we combined the two TNF^{low} bins by averaging for each sgRNA its read counts in the two bins. Next, we performed differential expression analysis on three biological repeats of TNF^{low} and TNF^{high} bins using the R package DESeq2 (Love et al., 2014) that fits a negative binomial generalized linear model (GLM). Normalization factors were provided to DESeq2 using non-parametric quantile normalization (R package EDASeq, 'betweenLaneNormalization'). Significant differences in abundance in TNF^{low} versus TNF^{high} bins were tested using a likelihood ratio test, testing the difference in deviance between a reduced model: counts ~ experiment and a full model: counts ~ experiment + TNF^{low}/TNF^{high}.

For the secondary screen, the three "low" TNF libraries were treated as technical replicates for the DE analysis, and averaged for the Z score analysis (see below). In addition in the secondary screen the default size factor normalization of DESeq2 was used and differential expression was tested using a Wald test.

Scoring sgRNA enrichment or depletion by Z-score analysis

As a second strategy to score sgRNAs whose levels are distinct between the TNF^{low} and TNF^{hi} cells, we used a Z-score based approach. First, we added one read to all the samples, and then quantile normalized the samples. We combined all low and high bins from the three experiments, into a single pair of TNF^{low} and TNF^{hi} bins, using the geometric mean of the quantile-normalized values. We performed the same procedure on all post-LPS, pre-LPS, and Input libraries. To control for the correlation of fold change to mean abundance, fold changes of TNF^{low} / TNF^{hi} were standard normalized in 12 bins of mean abundance (mean of TNF^{low} and TNF^{hi}), each containing ~10,000 guides. To collapse to gene level, the mean of the top four ranked sgRNAs was taken for positive regulators, and the bottom four ranked sgRNAs for negative regulators. Empirical *P*-values were calculated by randomly assigning sgRNAs to genes and false discovery rates (FDR) were assessed using the method (Benjamini and Hochberg 1995).

For the secondary library, we normalized each sample by the total number of reads and multiplied by 10^6. Because the secondary library is enriched for regulators, the fold changes of TNF^{low} / TNF^{hi} were standard normalized with respect to the non-targeting guides within each window (6 windows in total). We then averaged on all sgRNAs per gene, the non-targeting guides were randomly collapsed to “genes” (10 sgRNAs per “gene” to mimic the analysis for the targeting sgRNAs). The ranking in the secondary screen section in the **Results** is based on Z score of positive regulators, the FDR include the positive and negative regulators.

In both analysis methods we include only genes that had 4 or more sgRNAs that pass the abundance filter.

1471 sgRNAs perfectly mapped to more than one gene. 1302 genes are affected by this redundancy. Of these, for 434 genes, all sgRNAs map to an indistinguishable member(s) of a paralogous gene family. We report arbitrarily one of the genes names in **Tables S1-S4** and report the 434 genes names in **Table S5**.

For the remaining 868 genes, at least one sgRNA is multiply-mapped, leading to potential loss of sensitivity and confounding effects. We report these genes in **Table S5**.

Classification of known genes that have immune annotation

We analyzed five major databases of immune gene annotations: Immport (Bhattacharya et al., 2014), IRIS (Kelley et al., 2005), Immunome (Ortutay and Vihinen, 2006), MAPK-NFkB network (Lynn et al., 2008), and the TLR pathway as defined by KEGG (Kanehisa and Goto, 2000). Genes that are not included in any of those databases (**Table S1**) were related as "new" or "not previously annotated".

To define a core gene set known to regulate our model system, we chose the subset of KEGG's TLR pathway genes that can directly connect LPS to Tnf in the pathway map found at this link: http://www.genome.jp/kegg-bin/show_pathway?mmu04620. This gene set was used for **Figure 1E** and **Figure 2B**.

Identifying significant effects on protein expression

To assess the impact on marker protein expression by individual sgRNAs and the genes they target we used the following procedure. First, for each protein marker and sgRNA, we tested for a significant difference between the distribution of protein expression (from flow cytometry) measured for the sgRNA and the distribution of protein expression from all non-targeting sgRNAs within the same plate, using a KS-test and reporting the KS-statistic, D_n. We then signed the KS-statistic D by a one-sided Wilcoxon rank sum test. For each non-targeting sgRNA we determined an individual KS-statistic D_n using all non-targeting sgRNAs within the same plate as described above. To control for any plate effects, the KS-statistics within each plate were further standard normalized using the mean and standard deviations of the D (KS-statistic) values calculated for the non-targeting sgRNAs in that plate. Samples that had a cell count lower than 1,500 were excluded from further downstream analysis.

Next, we collapsed biological repeats of the same sgRNA using the mean of the Z-scored KS-statistic. High quality plates that included live / dead staining were favored over other plates; only when no measurement in the high quality plates was available for a given sgRNA, the measurements of the low quality plates were included. A tested sgRNA was considered a true positive regulator of Tnf if it passed the cutoff of -1.5 Z-score, which was determined using the Tnf Z-scores of the non-targeting sgRNAs.

Finally, true positive guides were collapsed to genes by taking the mean of the Z-scored KS-statistic across the sgRNAs, again favoring the high quality plates as we did for

collapsing biological repeats of the same guide. For **Figure 3A** and **Figure S3A**, we conservatively excluded genes if one sgRNA targeting the gene showed a significant effect on a marker (cutoff -1.5 Z-score) and the other sgRNA did not, and the absolute Z-score difference was >2.5. Five genes were filtered due to such discrepancies (Tnf, Gpkow, Pabpc1, Map3k8, Srpr).

Note, that since the distribution can be multi-modal and skewed in varied ways, we also manually visually inspected – independently and blindly to the computational analysis – the distributions in each individual experiment and each individual marker. There were four discrepancies between the automated and manual calls (Traf6, Akrin2, Ddx39b), and they therefore are not presented in **Figure 3A**.

RNA-Seq

BMDCs were infected with individual sgRNAs, expanded and differentiated in the presence of puromycin (from day 6 onward) in 96 well plates. At day 9, LPS was added for 2, 4 or 6 hours with or without Brefeldin (or not added at all – time point 0h). RNA was purified using Qiagen RNAeasy 96 Kit according to the manufacturer's instructions. The RNA was eluted in a volume of 50µl. For library construction we used the SMART-seq2 protocol (Picelli et al., 2013) in a 96 well plate format and with several modifications. 2µl of RNA sample per well were mixed with 2µl RT primer (10µM 5′-AAGCAGTGGTATCAACGCAGAGTACT30VN-3′), 2µl dNTP mix (10mM each, Agilent Technologies) and 2µl Recombinant RNase Inhibitor (RRI-Clontech). This mix was incubated for 3min at 72°C and immediately placed on ice. To perform reverse

transcription (RT) we added a mix of 1.5µl H_2O, 4µl Maxima buffer (ThermoFisher Scientific), 4µl Betaine (5M SIGMA-ALDRICH), 1.8µl MgCL2, 2µl TSO (10µM AAGCAGTGGTATCAACGCAGAGTACrGrG+G), 0.5µl RRI and 0.2µl Maxima H Minus Reverse Transcriptase enzyme (ThermoFisher Scientific). We incubated the RT reaction mix at 42°C for 90 min followed by 10 cycles of 50°C for 2 min, 42°C for 2 min, afterwards heat inactivated the enzyme for 15 min at 70°C. We used 11µl of the RT reaction for the PCR reaction by adding 12.5µl KAPA HiFi Hotstart (KAPA Biosystems), 1µl H_2O and 0.5µl of (10µM 5'-AAGCAGTGGTATCAACGCAGAGT-3′) primer under the following conditions: 98°C for 3 min, 14 cycles of (98°C for 15 sec, 67°C for 20 sec, 72°C for 6 min), final extension at 72°C for 5 min. The PCR product was used for library preparation with Nextera XT DNA Sample Preparation (Illumina) according to the manufacturer's instructions. Samples were combined and purified using Ampure XP Agencourt beads (Beckman Coulter) and sequenced on a Hi-Seq 2500 (Illumina), to generate paired-end 25bp reads. Each sample was sequenced to an average depth of four million reads (IQR-2.3 -5.5 million).

RNA-seq analysis

We created a Bowtie index based on the mm9 mouse reference genome, and then aligned paired-end reads directly to this index using Bowtie v 0.12.7 (Trapnell et al., 2009). Next, we ran RSEM v1.11 (Li and Dewey, 2011) with default parameters on these alignments to estimate expression levels. RSEM's gene level expression estimates (tau) were multiplied by 1,000,000 to obtain transcript per million (TPM) estimates for each gene. To transform expression levels to log-space, we took the log2(TPM+1). Sequencing

libraries that correlated poorly (Pearson $r<0.8$) with the majority of samples or had fewer than 500,000 expected counts across the transcriptome were removed from further analysis.

The log2(TPM+1) values were then quantile normalized, which reduced the coefficient of variation for each gene across samples. Without batch correction, samples separated strongly according to the experiment and plate in the first two principal components within a given time point. Batch correction was performed using the SVA package in R (Leek et al., 2012) using ComBat (Johnson et al., 2007). The primary known batch covariate was the plate on which the sample was processed. After batch correction, the effects associated with batch were attenuated.

To determine mRNAs whose expression is affected by knockout of individual genes, we first collapsed expression profiles from multiple sgRNAs that target the same gene, as long as those sgRNAs had expression profiles that were significantly correlated. To determine with sgRNAs had significantly correlated profiles, we compared their pair-wise linear (Pearson) correlation to a background distribution of Pearson correlation coefficients between non-targeting sgRNAs and all other sgRNAs within a time point. We then averaged the batch-corrected log2(TPM+1) data for all sgRNAs targeting the same gene whose pair-wise correlations exceeded the threshold of one standard deviation from the background distribution. Finally, we Z-transformed the expression profiles (collapsed from guides to genes) relative to the expression values for non-targeting sgRNAs at the same time point. We set a threshold for significance of the effect of a

perturbed gene on a target mRNA to a Z-score of four. We clustered the collapsed and Z-transformed profiles using hierarchical agglomerative clustering with complete linkage and a Pearson correlation (**Figure 3D**).

To identify genes that are differentially expressed between a set of experiments involving members of one module or complex vs. other modules or non-targeting controls (as per **Figure 4B-F**) we used differential expression analysis with the Wald test in the DESeq2 package (Love et al., 2014) with default parameters using the expected counts from RSEM. Batch correction was taken into account in the experimental design. Analysis of differential expression by complex/module was performed between the expression profiles from all samples transduced with sgRNAs targeting the complex to the expression of samples containing non-targeting sgRNAs collected at the same time point.

Paf1 and Rtf1 Immunopurification (IP) followed by quantitative mass spectrometry to identify interaction partners

For each IP 20 million unstimulated BMDCs (day 9) derived from C57BL/6J female mice were used. Paf1 IP was performed by using anti-Paf1 antibody (Bethyl Laboratories, A300-173A) and Rtf1 IP by using anti-Rtf1 antibody (Bethyl Laboratories, A300-178A). Control IPs were performed with a rabbit IgG control antibody (Bethyl Laboratories, P120-101). Each Paf1 or Rtf1 IP was always performed in parallel to a control IP and in two independent replicates.

BMDCs were harvested and washed twice with ice-cold PBS and lysed for 30 min in 400µl ice-cold lysis buffer (150mM NaCl, 50mM Tris/HCl pH 7.5, 1% IGPAL-CA-630 (Sigma, #I8896), 5% Glycerol, 2µg/mL aprotinin (Sigma, A6103), 10µg/mL leupeptin (Roche, #11017101001), 1 mM PMSF (Sigma, 78830). Lysates were centrifuged at 14,000*g* for 10 min. In parallel, 100µl of Protein G Dynabeads (Life Technologies) per IP were washed 3 times in 500µl lysis buffer. Cleared lysate, washed Protein G Dynabeads and 10µg of antibody were all mixed together in a 1.7ml Eppendorf tube and incubated on a rotator at 4°C overnight (16-18 hours). After overnight incubation, the supernatant was removed, the beads washed twice with 500µl ice-cold wash buffer (150mM NaCl, 50 mM Tris/HCl pH 7.5, 5% Glycerol) + 0.05% IGPAL-CA-630 (Sigma, #I8896) and two additional times with 500µl ice-cold wash buffer only. The beads were then incubated with 80µl urea/trypsin buffer (2M urea, 50mM Tris/HCl pH 7.5, 1mM DTT, 5µg/ml Trypsin (Promega)) for 1 hour at 25°C on a shaker (1,000 rpm) in order to release the bound proteins by an on-bead protein digest. Next, the supernatant was transferred to a new Eppendorf tube and the beads were washed twice with 60µl urea buffer (2M urea, 50mM Tris/HCl pH 7.5). The supernatant of the two washes and the on-bead digest were combined (total of 200µl), centrifuged at 5,000g in order to remove residual beads and the supernatant was further processed for mass spectrometry.

Disulfide bonds were reduced with 5mM dithiothreitol (DTT) and cysteines were subsequently alkylated with 10mM iodoacetamide. Samples were further digested by adding 0.5µg sequencing grade modified trypsin (Promega) at 25°C. After 16 h of digestion, samples were acidified with 1% formic acid (final concentration). Tryptic

peptides were desalted on C18 StageTips according to (Rappsilber et al., 2007) and evaporated to dryness in a vacuum concentrator.

Desalted peptides of the first repeat of the IPs (replicate 1) were labeled with the iTRAQ reagent according to the manufacturer's instructions (AB Sciex) and as previously described (Mertins et al., 2012). Briefly, 0.5 units of iTRAQ reagent were used per IP. Peptides were dissolved in 15µl of 0.5 M TEAB pH 8.5 solution and the iTRAQ reagent was added in 35µl of ethanol. After 1 h incubation the reaction was stopped with 100 mM Tris/HCl (pH 8.0). Differentially labeled peptides were mixed and subsequently desalted on C18 StageTips (Rappsilber, Mann, and Ishihama 2007) and evaporated to dryness in a vacuum concentrator. Peptides were reconstituted in 10µl 3% MeCN/0.1% formic acid. LC-MS/MS analysis was performed as previously described (Mertins et al., 2013).

Desalted peptides of the second repeat of the IPs (replicate 2) were labeled with the TMT10plex mass tag labeling reagent according to the manufacturer's instructions (Thermo Scientific) with small modifications. Briefly, 0.1 units of TMT10plex reagent was used per IP. Peptides were dissolved in 10µl of 50mM Hepes pH 8.5 solution and the TMT10plex reagent was added in 4.1µl of MeCN. After 1 h incubation the reaction was stopped with 1 µl 5% Hydroxylamine for 15 min at 25°C. Differentially labeled peptides were mixed and subsequently desalted on C18 StageTips (Rappsilber et al., 2007) and evaporated to dryness in a vacuum concentrator. Peptides were reconstituted in 20 ul 3% MeCN/0.1% formic acid. LC-MS/MS analysis was performed as previously described (Mertins et al., 2013).

All mass spectra were analyzed with MaxQuant software version 1.5.2.8 (Cox and Mann, 2008) using the mouse UniProt database (July 2014) (UniProt, 2015). MS/MS searches for the proteome data sets were performed with the following parameters: Oxidation of methionine and protein N-terminal acetylation as variable modifications; carbamidomethylation as fixed modification. Trypsin/P was selected as the digestion enzyme and 2 missed cleavages per peptide were allowed. The mass tolerance for precursor ions was set to 20 p.p.m. for the first search (used for nonlinear mass re-calibration) and 6 p.p.m. for the main search. Fragment ion mass tolerance was set to 20 p.p.m. For identification, we applied a maximum FDR of 1% separately on the protein and peptide level. We required 2 or more unique/razor peptides for protein identification and a ratio count of 2 or more for protein quantification per replicate measurement in at least one of the two replicates.

We calculated for each protein the log2 ratio between each candidate IP (Paf1 or Rtf1) over its control IP (rabbit IgG) for each replicate independently. We then subtracted for each replicate and IP the median of the distribution of the log2 transformed values (across all proteins that passed our filter: quantified in both replicates and in at least one replicate by two or more unique/razor peptides for protein identification and a ratio count of 2 or more for protein quantification) from the individual log2 ratios of each protein, to center the log2 ratio distribution around 0. Proteins with a log2 ratio > 0.8 (> 1.7 fold) in both replicate IPs were considered to be interactors.

Verification of the Paf1 and Auh interaction by Western blot

We performed Western plot on the cleared cell lysate (=Input) and the Protein G dynabeads after overnight incubation with the cell lysate and either Paf1 antibody or control rabbit IgG and the subsequent four washes (IP). We used anti-Paf1 antibody (Bethyl Laboratories, A300-173A) and anti-Auh antibody (ABCAM, ab155980).

DNA sequencing of cut site

To quantify the fraction of sequencing reads that reflect loss-of-function alleles we examined their alignments to the genomic target region. First, we excluded contaminating reads that do not have an exact match to at least one 20bp segment in the genomic target region. Second, we used Smith-Waterman local alignment and identified all mismatches, insertions and deletions (indels) in the read relative to the aligned portion of the genomic target region. We focused on indels, since the effect of mismatches on protein function is not easily predicted. We then calculated the combined length of the shift due to the remaining indels, *i.e.*, the total length of insertions minus the total length of deletions. Note that most reads contain only a single indel. All reads with indels whose combined length is not a multiple of three were defined as frame-shift reads and thus loss-of-function alleles, while all other non-excluded reads were defined as functional alleles.

Accession numbers

The RNA-Seq data is deposited in the Gene Expression Omnibus accession number GSE67164. The sgRNA sequencing data is deposited in http://www.broadinstitute.org/pubs/TNF_CRISPR_DCs/

The processed mass spectrometry data is reported in **Table S4** and raw mass spectrometry data is available upon request.

Supplemental References

Amit, I., Garber, M., Chevrier, N., Leite, A.P., Donner, Y., Eisenhaure, T., Guttman, M., Grenier, J.K., Li, W., Zuk, O.*, et al.* (2009). Unbiased reconstruction of a mammalian transcriptional network mediating pathogen responses. Science *326*, 257-263.

Benjamini, Y., and Hochberg, Y. (1995). "Controlling the false discovery rate: a practical and powerful approach to multiple testing". Journal of the Royal Statistical Society, Series B *57* (1): 289–300.

Bhattacharya, S., Andorf, S., Gomes, L., Dunn, P., Schaefer, H., Pontius, J., Berger, P., Desborough, V., Smith, T., Campbell, J.*, et al.* (2014). ImmPort: disseminating data to the public for the future of immunology. Immunologic research *58*, 234-239.

Chevrier, N., Mertins, P., Artyomov, M.N., Shalek, A.K., Iannacone, M., Ciaccio, M.F., Gat-Viks, I., Tonti, E., DeGrace, M.M., Clauser, K.R.*, et al.* (2011). Systematic discovery of TLR signaling components delineates viral-sensing circuits. Cell *147*, 853-867.

Cox, J., and Mann, M. (2008). MaxQuant enables high peptide identification rates, individualized p.p.b.-range mass accuracies and proteome-wide protein quantification. Nature biotechnology *26*, 1367-1372.

Doench, J.G., Hartenian, E., Graham, D.B., Tothova, Z., Hegde, M., Smith, I., Sullender, M., Ebert, B.L., Xavier, R.J., and Root, D.E. (2014). Rational design of highly active sgRNAs for CRISPR-Cas9-mediated gene inactivation. Nature biotechnology *32*, 1262-1267.

Garber, M., Yosef, N., Goren, A., Raychowdhury, R., Thielke, A., Guttman, M., Robinson, J., Minie, B., Chevrier, N., Itzhaki, Z.*, et al.* (2012). A high-throughput chromatin immunoprecipitation approach reveals principles of dynamic gene regulation in mammals. Molecular cell *47*, 810-822.

Johnson, W.E., Li, C., and Rabinovic, A. (2007). Adjusting batch effects in microarray expression data using empirical Bayes methods. Biostatistics *8*, 118-127.

Kanehisa, M., and Goto, S. (2000). KEGG: kyoto encyclopedia of genes and genomes. Nucleic acids research *28*, 27-30.

Kelley, J., de Bono, B., and Trowsdale, J. (2005). IRIS: a database surveying known human immune system genes. Genomics *85*, 503-511.

Langmead, B., Trapnell, C., Pop, M., and Salzberg, S.L. (2009). Ultrafast and memory-efficient alignment of short DNA sequences to the human genome. Genome biology *10*, R25.

Leek, J.T., Johnson, W.E., Parker, H.S., Jaffe, A.E., and Storey, J.D. (2012). The sva package for removing batch effects and other unwanted variation in high-throughput experiments. Bioinformatics *28*, 882-883.

Li, B., and Dewey, C.N. (2011). RSEM: accurate transcript quantification from RNA-Seq data with or without a reference genome. BMC bioinformatics *12*, 323.

Love, M.I., Huber, W., and Anders, S. (2014). Moderated estimation of fold change and dispersion for RNA-seq data with DESeq2. Genome biology *15*, 550.

Lutz, M.B., Kukutsch, N., Ogilvie, A.L., Rossner, S., Koch, F., Romani, N., and Schuler, G. (1999). An advanced culture method for generating large quantities of highly pure dendritic cells from mouse bone marrow. Journal of immunological methods *223*, 77-92.

Lynn, D.J., Winsor, G.L., Chan, C., Richard, N., Laird, M.R., Barsky, A., Gardy, J.L., Roche, F.M., Chan, T.H., Shah, N.*, et al.* (2008). InnateDB: facilitating systems-level analyses of the mammalian innate immune response. Molecular systems biology *4*, 218.

Martin, M. (2011). Cutadapt removes adapter sequences from high-throughput sequencing reads. EMBnet.journal 17, pp. 10–12.

Mertins, P., Qiao, J.W., Patel, J., Udeshi, N.D., Clauser, K.R., Mani, D.R., Burgess, M.W., Gillette, M.A., Jaffe, J.D., and Carr, S.A. (2013). Integrated proteomic analysis of post-translational modifications by serial enrichment. Nature methods *10*, 634-637.

Mertins, P., Udeshi, N.D., Clauser, K.R., Mani, D.R., Patel, J., Ong, S.E., Jaffe, J.D., and Carr, S.A. (2012). iTRAQ labeling is superior to mTRAQ for quantitative global proteomics and phosphoproteomics. Molecular & cellular proteomics : MCP *11*, M111 014423.

Ortutay, C., and Vihinen, M. (2006). Immunome: a reference set of genes and proteins for systems biology of the human immune system. Cellular immunology *244*, 87-89.

Picelli, S., Bjorklund, A.K., Faridani, O.R., Sagasser, S., Winberg, G., and Sandberg, R. (2013). Smart-seq2 for sensitive full-length transcriptome profiling in single cells. Nature methods *10*, 1096-1098.

Platt, R.J., Chen, S., Zhou, Y., Yim, M.J., Swiech, L., Kempton, H.R., Dahlman, J.E., Parnas, O., Eisenhaure, T.M., Jovanovic, M.*, et al.* (2014). CRISPR-Cas9 knockin mice for genome editing and cancer modeling. Cell *159*, 440-455.

Rappsilber, J., Mann, M., and Ishihama, Y. (2007). Protocol for micro-purification, enrichment, pre-fractionation and storage of peptides for proteomics using StageTips. Nature protocols *2*, 1896-1906.

Sanjana, N.E., Shalem, O., and Zhang, F. (2014). Improved vectors and genome-wide libraries for CRISPR screening. Nature methods *11*, 783-784.

Shalem, O., Sanjana, N.E., Hartenian, E., Shi, X., Scott, D.A., Mikkelsen, T.S., Heckl, D., Ebert, B.L., Root, D.E., Doench, J.G.*, et al.* (2014). Genome-scale CRISPR-Cas9 knockout screening in human cells. Science *343*, 84-87.

Trapnell, C., Pachter, L., and Salzberg, S.L. (2009). TopHat: discovering splice junctions with RNA-Seq. Bioinformatics *25*, 1105-1111.

UniProt, C. (2015). UniProt: a hub for protein information. Nucleic acids research *43*, D204-212.